P-021 NMR analyses of the protein-membrane interaction by using phosphoinositide-incorporated lipid-protein nanodiscs

Mariko Yokogawa[1], Naoki Yoshida[2], Yoshihiro Kobashigawa[1], Kenji Ogura[1], Kohsuke Harada[2] and Fuyuhiko Inagaki[1]
[1]Faculty of Advanced Life Science, Hokkaido University
[2]Graduate School of Life Science, Hokkaido University

[ABSTRACT]
Phosphoinositides (PIs) are crucial membrane components, and are involved in various cellular processes through interactions with their effector proteins. Recently, we have established a lipid-protein nanoscale bilayer (Nanodisc) containing PIs, which is suitable for studying protein-membrane interactions (Kobashigawa Y. *et al.*, *Anal. Biochem.*, (2011)). Here, we present further NMR applications of PIs-incorporated nanodiscs for studying protein-membrane interaction.

[INTRODUCTION]
Phosphoinositides (PIs) play important roles through the interaction with their effector proteins containing PI-binding domains, such as FYVE, PH, PX, ENTH. In our cell, seven distinct PIs are produced by phosphorylation of the hydroxy groups at positions of 3, 4, and/or 5 of the inositol ring. Specific recognitions of PIs by effector proteins are crucial for various cellular processes. Taking advantage of Nanodisc: a native-like membrane mimetic composed of lipid bilayers surrounded by two molecules of membrane scaffold protein (MSP), we have established Nanodisc containing PIs, which is hereafter referred to as PI-Nanodisc (Fig. 1), and demonstrated that they are useful for quantitative evaluation of the interaction between PIs and PI-binding proteins by pulldown assay and fluorescence polarization (Ref. 1). Here, further studies on the interaction between PI-binding protein and PI-Nanodisc were performed by using NMR, where the interaction between the FYVE domain of EEA1 and PI(3)P-Nanodisc was selected as a model of protein-membrane interaction.

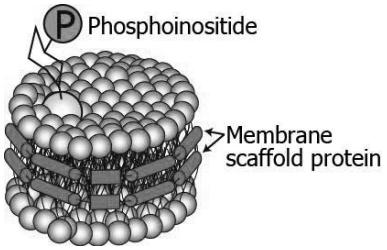

Fig. 1
Schematic representation of PI-Nanodisc.

[MATERIALS AND METHODS]
The FYVE domain of human EEA1 (residue number 1346-1411) was expressed in *E. coli* and purified to homogeneity. MSP was expressed in *E. coli*, purified, and mixed with lipid solution containing DMPC and PI(3)P solubilized by sodium deoxicholate. After the removal of detergent from the mixture of the lipid and MSP by using detergent absorbent beads, PI-Nanodisc was separated by size exclusion chromatography as a single elution peak.

NMR experiments were performed at 25°C in 10 mM Tris-HCl (pH 7.4), and 100 mM NaCl. In transferred cross-saturation (TCS) and titration experiments, 1 mM DTT was added to the sample. In paramagnetic relaxation enhancement (PRE) experiments, HSQC spectra were obtained both in the absence (paramagnetic) and presence (diamagnetic) of ascorbic acid.

Protein-membrane interaction, nanodisc, PI-binding domain

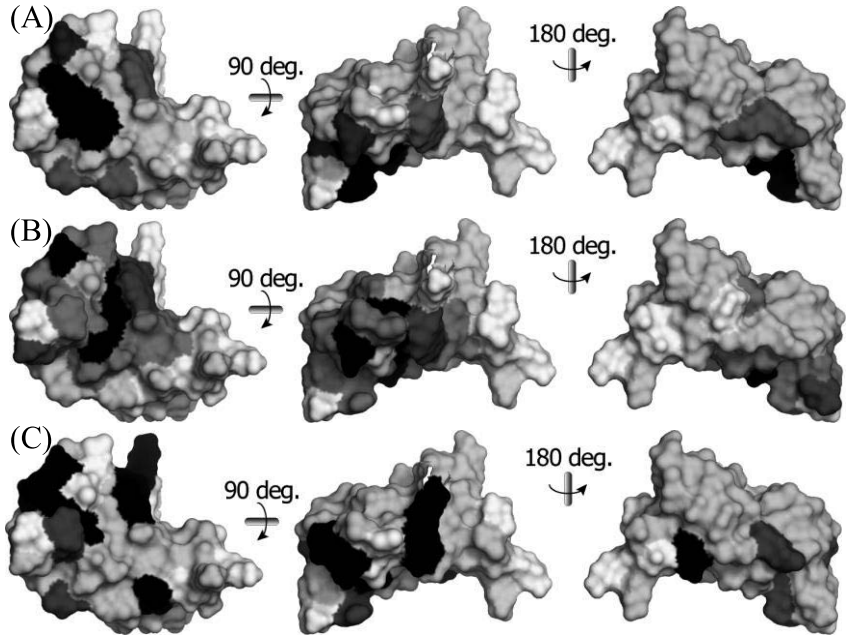

Fig. 2 Results of NMR experiments.
The results of (A) TCS, (B) titration, and (C) PRE experiments were mapped on the surface of EEA1 FYVE (PDB code: 1JOC). The strongly affected residues in each experiment upon binding to PI(3)P-Nanodisc were mapped in darker color, while residues excluded from the analyses were colored white. In the PRE experiment (C), both amide protons derived from main chain and side chain were utilized for the analysis. Left, middle, and right pictures represent rotations of an EEA1 FYVE molecule.

[RESULTS]

(1) Determination of PI(3)P-Nanodisc binding residues on EEA1 FYVE by TCS experiments.

TCS experiment was performed in the presence of PI(3)P-Nanodisc. As a control, those in the presence of PI(3)P-free nanodisc and in the absence of nanodisc were also performed. The residues with large intensity reduction only in the presence of PI(3)P-Nanodisc were located on the same side of the molecule, indicating the PI(3)P binding surface on EEA1 FYVE (Fig. 2 (A) left).

(2) Identification of the residues on EEA1 FYVE involved in the interaction with PI(3)P-Nanodisc by titration experiments.

Intensities of several signals derived from EEA1 FYVE were specifically reduced upon addition of PI(3)P-Nanodisc, indicating that these residues were involved in the direct binding of PI(3)P-Nanodisc and/or conformational change of EEA1 FYVE induced by the PI(3)P-Nanodisc binding (Fig. 2 (B)).

(3) Determination of the residues proximal to membrane surface by PREs observed from the paramagnetic spin-labeled lipid incorporated into PI(3)P-Nanodisc.

TEMPO-PC was introduced into PI(3)P-Nanodisc as a spin-label probe of membrane surface. PREs were observed for several signals including those derived from side chain amide protons, indicating their proximity of membrane surface in the complex (Fig. 2 (C))

[DISCUSSION]

Residues of EEA1 FYVE affected in each NMR experiment were mostly located on the same side of the molecule This is consistent with the previous report determined by using soluble PI(3)P analogue or detergent solubilized PI(3)P, suggesting that the binding site for PI(3)P embedded in lipid bilayers was successfully identified by using PI(3)P-Nanodisc. Therefore, PI-Nanodisc would be useful for studying various protein-membrane interactions at residue specific resolution under native-like membrane conditions.

[REFERENCE]

1. Kobashigawa Y., Harada K., Yoshida N., Ogura K., and Inagaki F., *Anal. Biochem.* (2011). **410**, 77-83

P-022 Role of protein fluctuation in determination of amyloid conformation,

Yumiko Ohhashi[1], and Motomasa Tanaka[1]
[1]Brain Science Institute, RIKEN

ABSTRACT
Aggregation-prone proteins often misfold into multiple distinct amyloid conformations. Although amyloid conformation is crucial factor to determine its toxicity or infectivity, the formation mechanism of diverse conformation remains unclear. Yeast prion Sup35, the [*PSI*$^{+}$] ptotein determinant, forms several type of amyloid with different conformations. Our previous studies demonstrated that restriction of fluctuation by non-native interaction in oligomer convert the amyloid core conformation. Here we show that the relationship between protein fluctuation and amyloid conformation in detail using NMR spectroscopy.

A ubiquitous feature of protein misfolding is that the same polypeptide can adopt structurally distinct fibrillar, β-sheet–rich aggregates termed amyloid fibers, with the specific misfolded conformation dictating its physiological impact. A notable example of this is the prion strain phenomenon, in which prion particles composed of the same protein cause distinct heritable states. Yeast prion Sup35 is also known to show several amyloid polymorphisms. Sup35 is translation termination factor composed of three domains (N, M, and C). A C domain carries translation termination function, and N, M domain is intrinsically disordered region with unknown function. Amyloid formation is caused in N domain and N-terminal of M domain.

The aim of this study is to investigate the mechanisms leading amyloid structural polymorphism using NM domain of Sup35 (Sup35NM).

Temperature dependent Sup35NM amyloid polymorphism

The Previous studies have shown that synthetic Sup35NM amyloids created at different temperatures adopt distinct conformations. Specifically, Sup35NM fibers formed at 4 °C and 37 °C shows fragile and rigid conformations, respectively. In our previous study, we discovered that this phenomenon is related to the temperature dependent formation of Sup35NM oliogmer. Oligomers are observed only at low temperature, and it works as a scaffold of nucleation.

The temperature-dependent formation of Sup35NM oligomer was readily monitored by NMR spectroscopy. A large fraction of the peaks in the HSQC spectrum of Sup35NM disappeared at low temperature because of the slow tumbling rate of oligomeric species (Figure 1). From these spectra, we estimated the core of oligomeric form and compared to the core of amyloid form measured by Mass spectrometry. Then, it was shown that the core of amyloid formed at low temperature avoided oligomer core region (Figure 2).

Amyloid, Sup35, Fluctuation

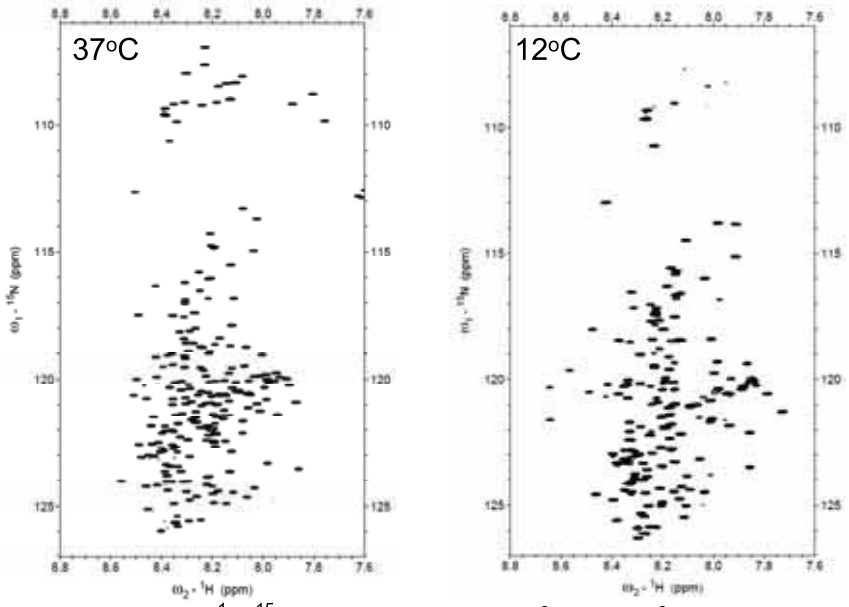

Figure 1. ^{1}H-^{15}N HSQC spectra at 37°C and 12°C

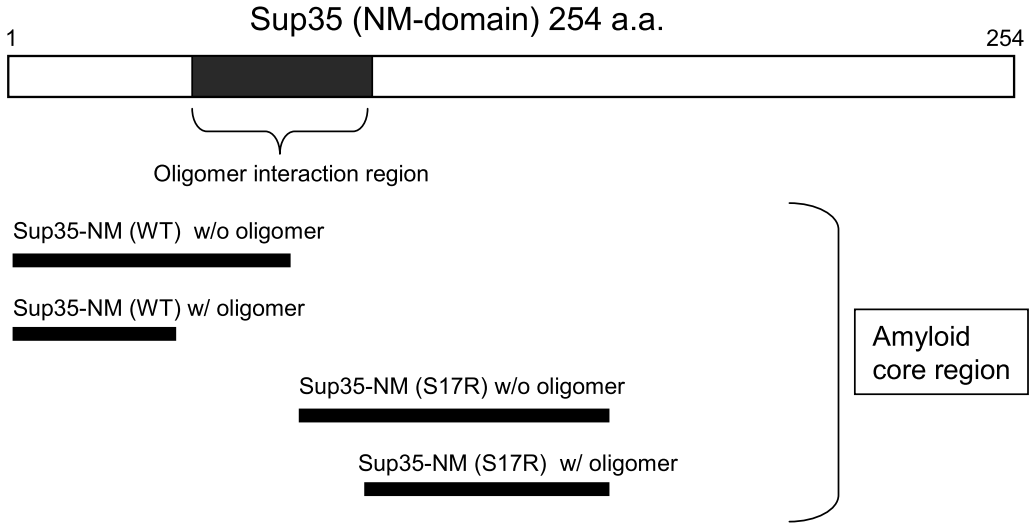

Figure 2. Oligomer and Amyloid core region of Sup35NM WT and S17R mutant.

Mutation dependent Sup35NM amyloid polymorphism

Previous report have shown that Sup35NM point mutation S17R change the yeast phenotype in [*PSI*$^{+}$] system. Therefore we examined the amyloid core region of S17R by mass spectrometry, and found surprising jump of region (Figure 2). Because S17R amyloid conformation can propagate to WT easily through the seeding reaction, we considered there are two intrinsic amyloid core possibilities in Sup35NM. We were able to get the evidence of this phenomenon by examining the fluctuation of the monomer Sup35NM.

P-023 Low-lying excited state of prion protein directly linked to pathogenic conversion

Yuji O. Kamatari[1], Keiichi Yamaguchi[2] and Kazuo Kuwata[2]
[1]Life Science Center, Gifu University,
[2]United Graduate School of Drug Discovery and Medical Information Sciences, Gifu University.

Conformational conversion of the cellular form of prion protein (PrP^{C}) to the scrapie form (PrP^{Sc}) plays a central role in the pathogenesis of transmissible spongiform encephalopathies. However, the precise mechanism of the conversion from PrP^{C} to PrP^{Sc} is still unknown. Recently, we have characterized metastable states of the PrP^{C} using a high-pressure NMR (1) and NMR relaxation (2) studies. Especially, the NMR relaxation studies revealed that slow fluctuation on a time scale of micro- seconds to milliseconds occurs at the corresponding regions, indicating the conformational rearrangements occurring between the native and the sparsely populated high-energy states or low-lying excited states of PrP^{C}. In our previous studies, we also discovered a chemical compound, GN8 and its derivatives, to stabilize the PrP^{C} conformation and identified the hot spots to stop the pathogenic conversion based on the binding site of the chemical compounds (3-5).

In this study, in order to identify the interaction sites of PrP^{C} with PrP^{Sc} in its pathogenic conversion, we observed in vitro conversion process using NMR. In vitro conversion method using a recombinant protein has been reported (6) and we have modified the scheme for NMR observation. First, we mixed ^{15}N-labelled recombinant mouse prion protein mPrP(23-231) with the brain homogenate (BH) of PrP^{Sc} infected mice or the BH of mock-infected normal mice and incubed the products at pH4.5 at 37 ºC. At a few weeks after mixing, we could not see any difference between the HSQC spectra. However, after a few months, we could clearly observed the differences in spectra. Western blot analysis showed that levels of protease K-resistant components significantly increased in the preparations with infected BH compared to those with normal BH. Residues that have chemical shift changes in this experiment are included in the hot spots identified by the anti-prion compounds. Low-lying excited state observed here seem to be directly linked to pathogenic conversion, designated to PrP^{Ex}.

In order to characterize the interaction between prion protein and anti-prion compounds, we measured the chemical shift differences between HSQC spectra with and without compounds. Chemical shifts of several residues changed significantly upon binding with GN8 derivatives. The binding sites essentially covers PrP^{Sc} susceptible sites shown above. Amplitudes of chemical shift perturbations dramatically increased with decreasing IC_{50}, although the distributions of the chemical shift perturbations over residue number are essentially unchanged. This result suggests that increase in chemical shift perturbation can be attributed to an increase in bound population in PrP^{C} or an increase in binding affinity between PrP^{C} and compounds.

In Fig. 1, we illustrate the possible working mechanism of the compounds act as medical chaperone. Native ensemble of prion protein is in equilibrium of exchange between PrP^{C} and PrP^{Ex} and population of PrP^{Ex} is quite small in a healthy condition. PrP^{Ex} is sticky and flexible and located

at an entrance to the pathogenic conversion pathway, and its population is significantly increased by the interactions with PrP^{Sc} at the PrP^{Sc} susceptible sites. PrP^{Ex} would be further altered to the intermediate state, PrP* (7) which is located between PrP^{Ex} and PrP^{Sc} on the conversion pathway. PrP* in a hetero-dimer would be eventually converted to PrP^{Sc} catalyzed by PrP^{Sc}, which act as a "template". While in the presence of compounds, it is physically impossible for PrP^{Ex} to contact with PrP^{Sc} due to intervention by the compound, because the binding regions of the compounds correspond to the interaction sites between PrP^{Ex} and PrP^{Sc}. Since PrP^{Sc} is degraded in vivo in long time scale, the population of PrP^{Sc} is consequently gradually reduced.

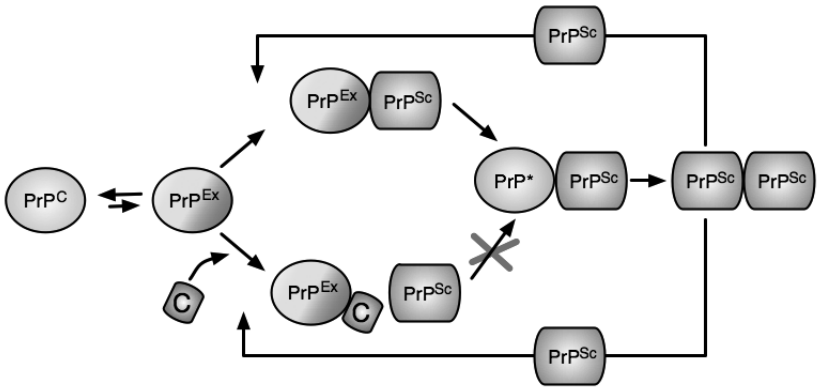

Fig. 1 An action mechanism of compounds act as medical chaperone.

In summary, we discovered a low-lying excited state of a prion protein locates at the entrance to conversion pathway (PrP^{Ex}). This report provides clear evidence of the early intra-molecular events that occur in the pathogenic conformational conversion in prions. This knowledge could be further applied to discover novel or more potent therapeutic candidates for human prion diseases.

References

1. Kuwata K et al., Biochemistry 41, 12277, 2002.
2. Kuwata K et al., Biochemistry 43, 4439, 2004.
3. Kuwata K et al., Proc Natl Acad Sci U S A 104, 11921, 2007.
4. Hosokawa-Muto J et al., Antimicrob. Agents Chemother. 53, 765, 2009.
5, Kimura T et al., Bioorg Med Chem Lett. 21, 1502, 2011.
6. Atarashi R et al., Nature Methods 4, 645, 2007.
7. Cohen FE et al., Science 264, 530, 1994.

low-lying excited state, prion, in vitro conversion, drug discovery

P-024 Structural studies of tubulin tyrosine ligase 1.

Kunimichi Saeki[1], Ryoko Maesaki[2] , Yutaka Ito[1],Toshio Hakoshima[2], and Masaki Mishima[1]
[1]Graduate school of science and engineering, Tokyo Metropolitan University
[2]Graduate school of Bioscience NAIST

Tubulin tyrosine ligase (TTL) is thought to play a crucial role for microtubule dynamics. It adds tyrosine to the C-terminal end of α-tubulin, and this is one of the key modifications of microtubule. Toward the understanding the detail of the tyrosination, we are trying to determine the TTL structure. We have optimized the buffer and the other conditions monitoring NMR spectrum. Further, we are trying to obtain solubility enhanced mutants suitable for structural analyses. We repot high-throughput system to prepare solubility enhanced mutants using GFP-fusion and random PCR technique.

【Introduction】

Microtubule consists of the hetero dimer units, α-tubulin and β-tubulin. CLIP170 and EB1 proteins play important role for elongation and stabilization of microtubule. It is known that CLIP170 protein recognizes tyrosine at the C-terminal end of α-tubulin. CLIP170 binds to the C-terminus of α-tubulin, accumulates at plus end of microtuble and promotes its polymerization. Thereafter, tyrosine at C-terminal end is cleaved by carboxypeptidase and CLIP170 detaches from α-tubulin. Tubulin tyrosine ligase (TTL) adds tyrosine to the C-terminal end of α-tubulin, thus CLIP170 can bind again and released α-tubulin is recycled for polymerization. This tyrosination is one of the key modifications to regulate microtube dynamics.

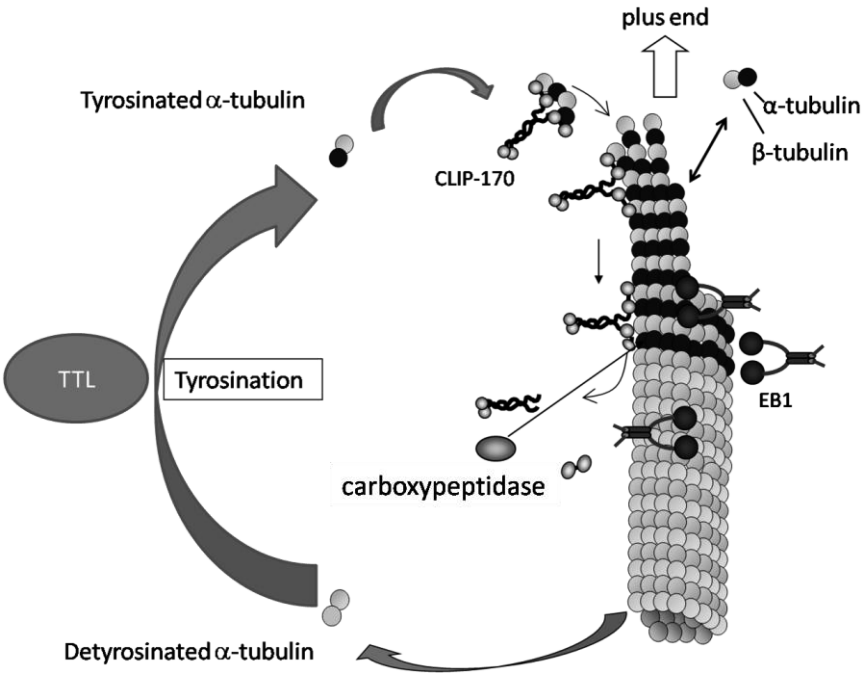

【^{1}H-^{15}N TROSY spectrum of TTL after optimization】

We could not obtain well dispersed signals possibly due to purified TTL forms aggregation at high concentration when we measured ^{1}H-^{15}N TROSY(Fig.2a). We next examined condition of the buffer. We optimized the conditions monitoring TROSY spectra. As a result, stability of TTL and quality of the spectrum were improved (Fig.2b). Further, we measured TTL- AMPPCP complex

TTL, enzyme

to check whether NMP binding improve enhance the solubility or not (Fig.2c). We found that high salt concentration is required for the solubility of TTL, and TTL-AMPPCP complex did not contribute the solubility. We therefore try to obtain solubility enhanced mutants suitable for structural analyses.

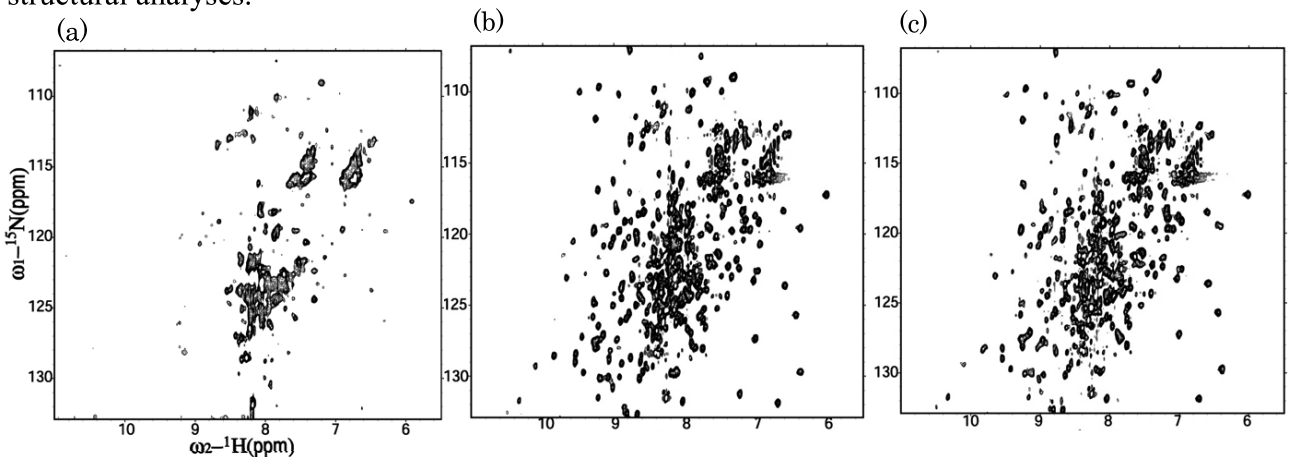

Fig.2 ^{1}H-^{15}N TROSY spectrum of TTL
(a) 0.25 mM TTL, 50 mM Bis-Tris (pH 7.0), 50 mM KCl, 0.5 mM DTT
(b) 0.49 mM TTL, 50 mM Bis-Tris (pH 6.0), 200 mM KCl, 1 mM $MgCl_2$, 0.5 mM DTT
(c) 0.49 mM TTL, 50 mM Bis-Tris (pH 6.0), 200 mM KCl, 1 mM $MgCl_2$, 1 mM AMPPCP, 0.5 mM DTT

【Examination of stable mutant of TTL】

We have made high-throughput monitoring system using GFP-fusion protein. We designed TTL-GFP plasmid using pBADuv which is inducible on plate including arabinose and GFP-TTL plasmid using pET151 vector which is inducible by IPTG. Since TTL formed inclusion body when it was induced at 37 ºC, we expected that fluorescence of the colony includes GFP-TTL was attenuated due to TTL in contrast to the colony which include only GFP showed clear fluorescence. As a results we confirmed this phenomenon. We then confirmed that the colony in expressed wild type GFP-TTL showed moderate fluorescence when TTL folded into native forms by moderate induction by lowering the temperature to 20 ºC.

To facilitate the through-put, we introduced random PCR technique. We generated a randomly mutated template using random PCR technique and then amplified it and cloned to expression vector as GFP-fusion protein. Currently, we are trying to find the solubility enhanced mutants using this system.

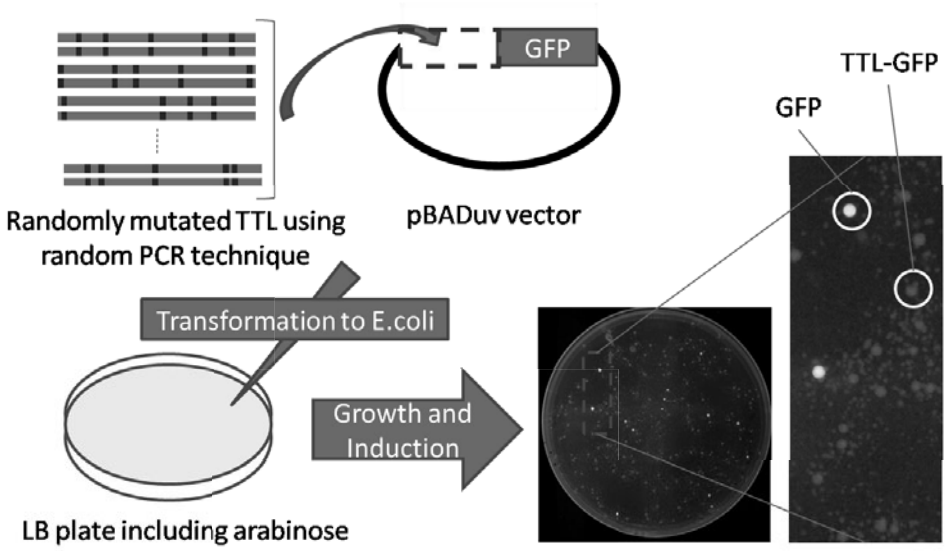

Fig.3 Scheme of monitoring system using GFP

P-025 Structural analysis for 85 kDa protein complex, general transcription factor TFIIE by NMR spectroscopy

Masahiko Okuda[1], Yoshihito Moriwaki[1], Masayuki Kataoka[1], Aritaka Nagadoi[1], Aki Tanaka[2], Yoshiaki Ohkuma[2] and Yoshifumi Nishimura[1]

[1]Graduate School of Nanobioscience, Yokohama City University, Japan
[2]Graduate School of Medicine and Pharmaceutical Sciences, University of Toyama, Japan

[ABSTRACT]
In eukaryotes, the transcription initiation of protein coding genes is performed by RNA polymerase II and general transcription factors, including TFIIE. Human TFIIE is a heterodimer consisting of α (50 kDa, 439 aa) and β (34 kDa, 291 aa) subunits. Here, we have analyzed the solution structure of the whole TFIIE molecule. We have identified NMR signals of the second half of TFIIEα and the N- and C-terminal regions of TFIIEβ, in addition to the central core domains of both subunits and TFIIEα C-terminal acidic domain. We will present the structure of the second half of TFIIEα in the whole TFIIE molecule.

[INTRODUCTION]
RNA Polymerase II (Pol II) is responsible for transcription of protein-coding genes in eukaryotes. Although Pol II is the complicated enzyme comprising 12 subunits, it alone is unable to initiate transcription. Transcription initiation by Pol II requires at least five proteins; TFIIB, TFIID, TFIIE, TFIIF, and TFIIH. These proteins are collectively known as general transcription factors. Pol II and general transcription factors assemble on a promoter DNA to form transcription pre-initiation complex (PIC). In the PIC formation, TFIIE recruits TFIIH into the PIC. After that, the double-stranded DNA around a transcription start site is melt into a single-stranded form by TFIIH. At the promoter melting, TFIIE binds the region where it is needed to initiate the melting and assists the formation of open complex. Following the extensive phosphorylation by TFIIH of the C-terminal domain (CTD) of Rpb1, a largest subunit of Pol II, the activated Pol II releases all general transcription factors expect for TFIIF and proceeds to transcription elongation. Upon the promoter clearance, TFIIE increases the CTD kinase activity of TFIIH. Thus, TFIIE and TFIIH have significant function in transcription initiation and the transition to elongation.

To elucidate the transcription initiation mechanism, structural information on the PIC at molecular level is indispensable. Based on so far determined structures, we can see the detail structural model of the partially forming PIC; TBP (a subunit of TFIID)-promoter DNA-Pol II-TFIIB complex. To complete the model, further structural information of the other general transcription factors including TFIIE is necessary.

We have established that human TFIIE is a heterodimer consisting of α (50kDa, 439aa) and β (34kDa, 291aa) subunits [1]. Using NMR we have already determined the structures of each isolated central core domain of TFIIE α [2] and β [3] subunits, in addition to the isolated C-terminal acidic domain of TFIIEα [4] and its bound form with the PH domain of TFIIH p62 subunit [4] (Figure 1). The core domain of TFIIEα consists of one α helix and six β-strands, showing novel

features distinct from previously determined zinc-binding structures. The core domain of TFIIEβ is a winged helix domain consisting of a three-helix bundle and a C-terminal β hairpin. Based on its structure we revealed that the TFIIEβ core domain is a double stranded DNA-binding domain. The acidic domain of TFIIEα holds a globular structure with a long disordered N-terminal tail, which is responsible for the interaction with the PH domain of TFIIH p62 subunit. Here, we have analyzed the NMR structure of the whole TFIIE molecule (TFIIEαβ complex), comparing with the structures of the isolated domains.

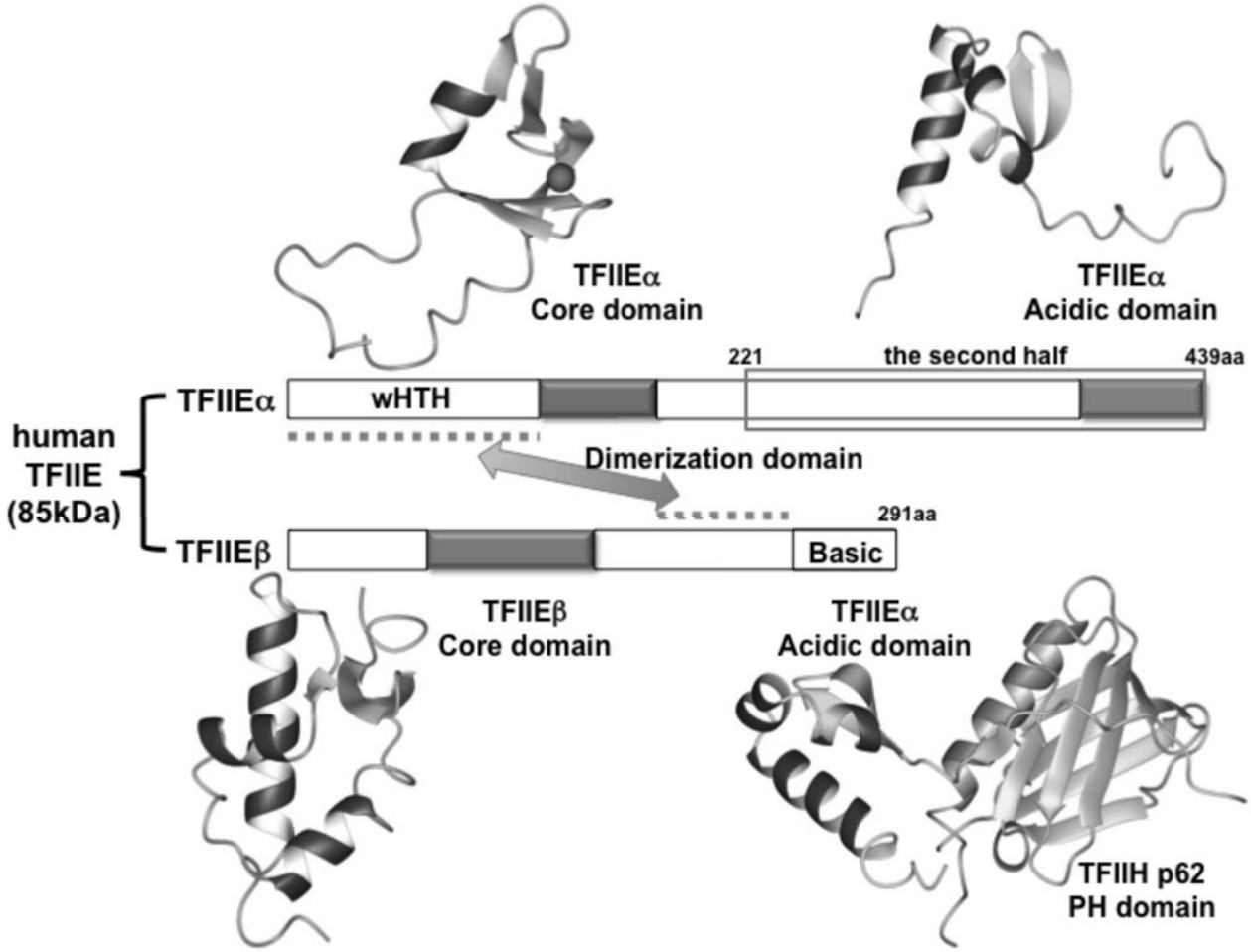

Figure 1 Isolated domain structures of human TFIIE.

[RESULTS & DISCUSSION]

We first established co-expression system for the whole TFIIE in *E. coli*. The genes encoding human TFIIEβ and TFIIEα were subcloned into the pETDuet-1 vector (Novagen), respectively, making the co-expression vector for the complex of the N-terminal histidine-tagged TFIIEβ and TFIIEα. In this system, TFIIEβ was more excessively expressed than TFIIEα, so that we could obtain TFIIEαβ and TFIIEβ at once. Both proteins had low solubility in standard NMR buffers, but in the buffer containing high salt concentration (500 mM and above NaCl) ~270 μM of the whole TFIIE and ~190 μM of TFIIEβ could be dissolved.

In the whole TFIIE molecule the perdeuterated ^{13}C, ^{15}N labeled sample gave ~380 backbone signals, which correspond to 52 % of the total residues, on the 2D ^{1}H,^{15}N-TROSY spectrum. We assigned 320 signals, or 84% of the observed signals (Figure 2). We identified almost signals of the

second half of TFIIEα, and the N- and C-terminal basic regions of TFIIEβ. The central domains of TFIIEα and TFIIEβ were partially identified. Any signals from the N-terminal region of TFIIEα, and the region between the central core domain and the C-terminal basic region of TFIIEβ were not observed. These two regions have been shown to be the dimerization domain (Figure 1).

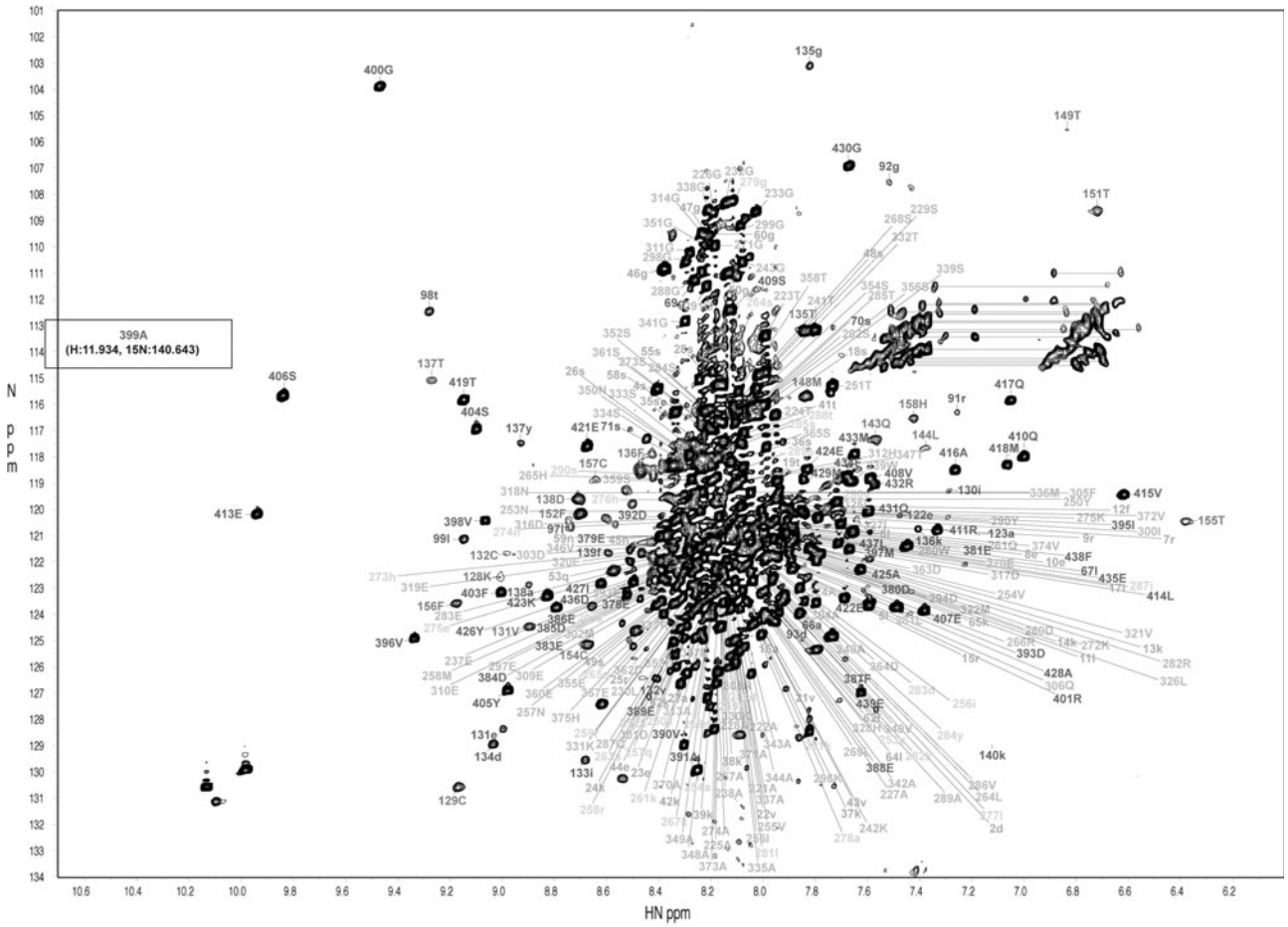

Figure 2　2D ^{1}H,^{15}N-TROSY spectrum of the whole TFIIE (TFIIEαβ).

In the TFIIEβ alone, the perdeuterated ^{13}C, ^{15}N labeled sample gave ~220 backbone signals corresponding to 75 % of the total residues on the 2D ^{1}H,^{15}N-TROSY spectrum. We assigned ~190 signals, or 86 % of the observed signals (Figure 3). We identified the signals of the N-terminal and the C-terminal basic regions in addition to the central core domain. The signals from the dimerization domain were not observed even in TFIIEβ alone.

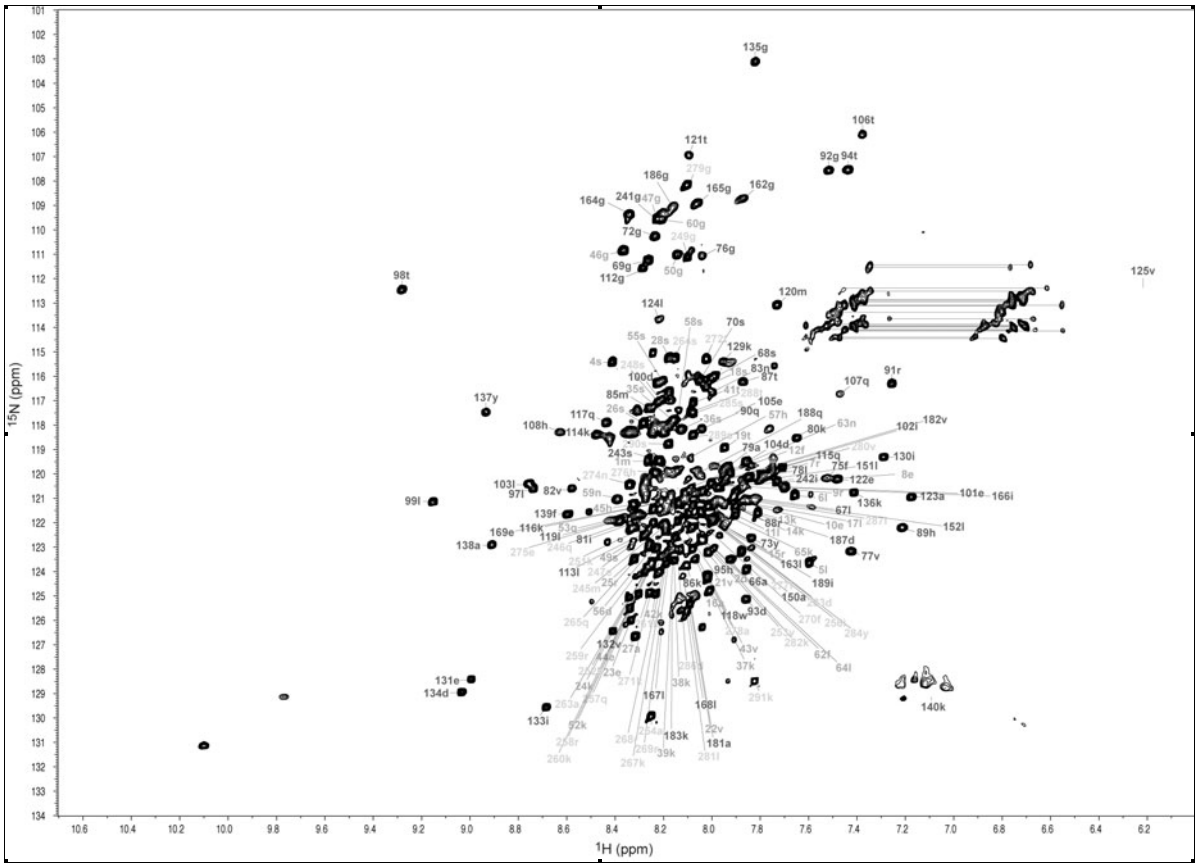

Figure 3 2D ^{1}H,^{15}N-TROSY spectrum of the TFIIEβ.

Chemical shift differences of TFIIEβ between the free form and the complex form were very small. Such very small chemical shift differences were also seen in the comparison of the chemical shift values of each three domain: TFIIEα core domain, TFIIEα acidic domain, and TFIIEβ core domain, between in the isolated form and in the whole TFIIE. Although the assigned signals are limited, the structures of three domains in the whole TFIIE would be identical to the structures of each isolated domain.

We have attempted to determine the structure of the second half of TFIIEα in the whole TFIIE. To address this, we have established the preparation system for a Stereo-Array Isotope Labelling (SAIL) TFIIE and used the sample of the complex between SAIL-TFIIEα and perdeuterated TFIIEβ besides the protonated or perdeuterated ^{13}C, ^{15}N labeled TFIIE. The present structure suggests that almost second half of TFIIEα excluding the acidic domain are disordered. We confirmed that this is true by measuring backbone amide ^{15}N spin relaxation (longitudinal and transverse relaxation rates, R1 and R2, and steady-state ^{15}N-{^{1}H} NOE) for the whole TFIIE.

This study reveals that TFIIE possesses an elongated structure consisting of small domains linked by the flexible long linkers.

[REFERENCES]

[1] Itoh et al., *PROTEINS*, 61, 633-641 (2005), [2] Okuda et al., *J. Biol. Chem.*, 279, 51395-51403 (2004), [3] Okuda et al., *EMBO J.*, 19, 1346-1356 (2000), [4] Okuda et al., *EMBO J.*, 27, 1161-1171 (2008)

Protein, Complex, 85 kDa

P-026 Relationship between ^{13}C NMR shift of Fe-bound CO and electron density of heme

Tomokazu Shibata[1], Ryu Nishimura[1], Masashi Fukaya[1], Hulin Tai[1], Takashi Matsuo[2], Shun Hirota[2], Akihiro Suzuki[3], Izumi Ishigami[4], Takashi Ogura[4], Saburo Neya[5], and Yasuhiko Yamamoto[1]
[1]Department of Chemistry, University of Tsukuba, [2]Graduate School of Materials Science, Nara Institute of Science and Technology, [3]Department of Materials Engineering, Nagaoka National College of Technology, [4]Graduate School of Life science, University of Hyogo, [5]Graduate School of Pharmaceutical Sciences, Chiba University

ABSTRACT Functional regulation of myoglobin (Mb) is thought to be achieved through the heme environment furnished by nearby amino acid residues, and electron density of heme Fe atom (ρ_{Fe}). In order to elucidate the effect of the ρ_{Fe} value on the nature of the coordination bond between heme Fe atom and carbon monoxide (CO) in Mb, we have performed the substitution of strongly electron-withdrawing perfluoromethyl (CF_3) group(s) as heme side chains(s). We demonstrated that ^{13}C NMR signal of ^{13}CO bound to Mb exhibits upfield shift with decreasing the ρ_{Fe} value due to the CF_3 introduction, and that the upfield shift of the ^{13}CO signal correlates well with the stretching frequencies of the Fe-C and C-O bonds of the Fe-CO fragment.

INTRODUCTION Myoglobin (Mb) is an oxygen (O_2) storage protein of molecular weight of about 17 kDa. We have recently demonstrated that the O_2 affinity of Mb is regulated by the electron density of the heme Fe atom (ρ_{Fe}) in a fashion that the O_2 affinity of the protein decreases with decrease in the ρ_{Fe} value due to an increase in the O_2 dissociation rate[1]. In contrast to the O_2 binding to Mb, the carbon monoxide (CO) affinity and the CO dissociation rate of the protein were found to be essentially independent of the ρ_{Fe} value. In this study, we investigated the effect of the ρ_{Fe} value on the nature of the Fe-CO binding in the protein through analysis of the relationship between the ρ_{Fe} value and ^{13}C NMR signal of ^{13}CO bound to the protein as well as the stretching frequencies of the Fe-C and C-O bonds of the Fe-CO fragment, measured by resonance Raman spectroscopy. The study demonstrated that the Fe-C bond strength decreases with decreasing the ρ_{Fe} value. Considering the negligible effect of the ρ_{Fe} value of the CO binding properties of the protein, the alteration of the Fe-C bond strength through the ρ_{Fe} value was likely to be too small to be reflected in the functional properties of the protein.

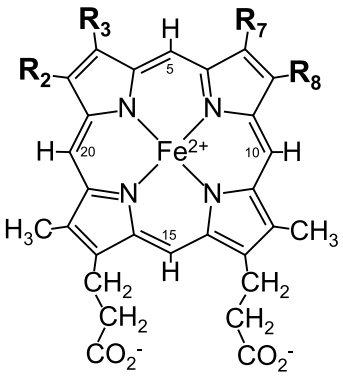

Fig. 1. The structures for hemes used in study,
Proto ($R_2 = R_7 = CH_3$, $R_3 = R_8 = CH{=}CH_2$), Meso ($R_2 = R_7 = CH_3$, $R_3 = R_8 = C_2H_5$), DMD ($R_2 = R_3 = R_7 = R_8 = CH_3$), 7-PF ($R_2 = CH_3$, $R_3 = R_8 = C_2H_5$, $R_7 = CF_3$), and 2,8-DPF ($R_2 = R_8 = CF_3$, $R_3 = R_7 = CH_3$).

RESULTS AND DISCUSSION

ρ_{Fe} Estimation. We introduced strongly electron-withdrawing perfluoromethyl (CF_3) group(s), as heme side chain(s), for large and stepwise alterations of the ρ_{Fe} value. Non-native hemes (Fig. 1) were synthesized according to the literatures, and then were incorporated into the protein using a technique known as the Mb reconstitution. The ρ_{Fe} value was estimated on the basis of the equilibrium constant (pK_a) of the so-called "acid-alkaline transition" of the oxidized

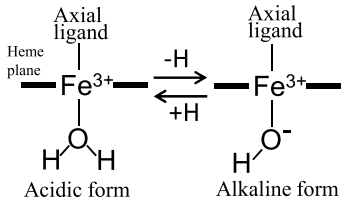

Scheme 1. Acid-alkaline transition in metMb.

Keywords: Myoglobin, heme, Fe-bound ^{13}CO shift, heme electronic structure

protein (Scheme 1). A decrease in the ρ_{Fe} value due to the CF_3 substitution should lower the H^+ affinity of Fe-bound OH^- in the alkaline form, which results in a decrease in the pK_a value. Indeed, comparison of the pK_a values among the proteins indicated that the introduction of one CF_3 group decreases the value by ~1 pH unit.

^{13}C NMR signal of ^{13}CO bound. ^{13}C NMR signals of ^{13}CO bound to the proteins possessing various hemes are shown in Fig. 2. The signals were observed at ~207 ppm[2], and the signal for a heme with smaller pK_a value exhibited larger upfield shift. The plots of the ^{13}CO shifts against the pK_a values of the hemes can be represented by a straight line (Fig. 3), indicating a close correlation between the ρ_{Fe} value and the ^{13}CO shift.

Stretching vibration of the Fe-C and C-O bonds of the Fe-CO fragment. The wavenumbers for the stretching vibration of the Fe-C and C-O bonds (ν_{Fe-C} and ν_{CO}, respectively) have been measured using resonance Raman spectroscopy. The plots of the ^{13}CO shifts against the ν_{CO} value demonstrated a close correlation between the ^{13}CO shifts and the C-O bond strength (Fig. 4), in a fashion that the C-O bond strength increases with decreasing the ρ_{Fe} value. This result can be interpreted in terms of a resonance between the two canonical forms (Scheme 2) [3]. With the CF_3 substitution, left form is expected to be stabilized relative to right form as a result of compensation for a decrease in the ρ_{Fe} value. Consequently, the bond order for the Fe-bound CO is expected to increase with decreasing the ρ_{Fe} value, leading to an increase in the ν_{CO} value. In contrast, the Fe-C bond order is expected to decrease with decreasing the ρ_{Fe} value, and hence the Fe-C bond becomes weaker with the CF_3 substitution. This interpretation was completely confirmed by DFT calculations carried out on model systems (Details to be included in the poster).

Relationship between the ρ_{Fe} value and the Fe-CO bond strength. Thus the Fe-C and C-O bonds were found to be affected by the ρ_{Fe} value. But the kinetic measurements indicated that the CO dissociation rate of the protein was independent of the CF_3 substitution. Since the coordination of CO to the heme Fe is inheritably strong, the alteration in the bond strength exerted by changing the ρ_{Fe} value is likely to be too small to be reflected in the protein function.

CONCLUSION

The study revealed that, the Fe-C bond becomes weaker with decreasing the ρ_{Fe} value, and consequently, ^{13}C NMR signals of the ^{13}CO bound exhibits upfield shift in the protein possessing lower pK_a value.

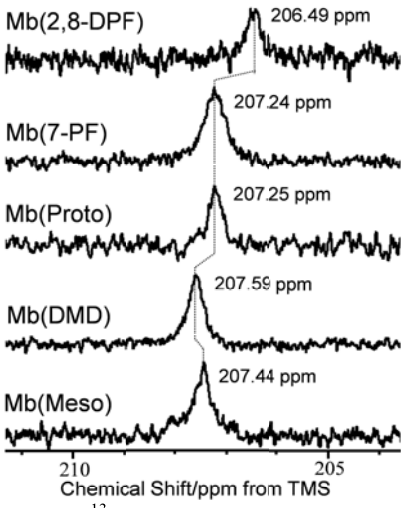

Fig. 2. ^{13}C NMR signals of heme Fe-bound ^{13}CO of various Mbs at pH 7.4 and 25°C.

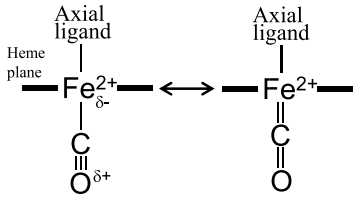

Scheme 2. Resonance electronic structures of CO bound to Mb.

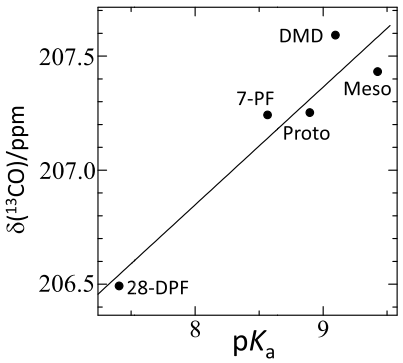

Fig. 3. Plots of the pK_a values against the ^{13}CO shift ($\delta(^{13}CO)$).

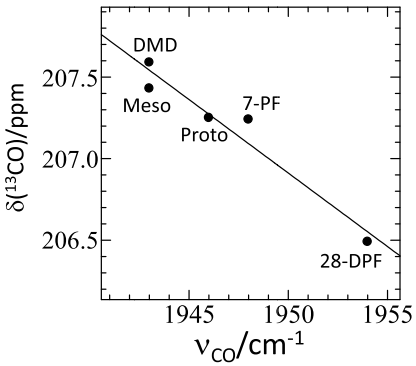

Fig. 4. Plots of the wavenumber of CO stretching bound to Mb (ν_{CO}) against the ^{13}CO shift ($\delta(^{13}CO)$) .

REFERENCES:[1] T. Shibata *et al.*, *J. Am. Chem. Soc.* 132, 6091–6098(2010). [2]R. B. Moon & J. H. Richards, *J. Am. Chem. Soc.* 94, 5093-5095(1972). [3]C. G. Kalodimos *et al., J. Inorg. Biochem.* 79, 371-380(2000).

P-027 Novel interaction mode of Atg8 with the extreme C-terminal region of Atg7

Hiroyuki Kumeta[1], Kenji Satoo[2], Nobuo N Noda[1,3], Yuko Fujioka[1,3], Kenji Ogura[1], Hitoshi Nakatogawa[4], Yoshinori Ohsumi[4], Fuyuhiko Inagaki[1,2]
[1]Department of Structural Biology, Faculty of Advanced Life Science, Hokkaido University. [2]Department of Structural Biology, Graduate School of Life Science, Hokkaido University. [3]Institute of Microbial Chemistry, Tokyo. [4]Frontier Research Center, Tokyo Institute of Technology.

ABSTRACT
Atg8 is a ubiquitin like protein required for autophagosome formation and conjugated to phosphatidylethanolamine by Atg7 (E1-like enzyme) and Atg3 (E2-like enzyme). It has been reported that the C-terminal region of Atg7 is critical for Atg8 activation. Moreover, we found that the initial recognition of Atg8 is predominantly mediated by the C-terminal 13 residues of Atg7, which is essential for formation of Atg7~Atg8 thioester intermediate. Here, we present the solution structure of Atg8 complexed with the extreme C-terminal region of Atg7.

[Introduction]

Autophagy is an evolutionarily conserved bulk degradation system that plays important roles in a number of biological processes and diseases, such as neurodegeneration. An autophagy essential protein, Atg7 is an E1-like enzyme that activates and forms a thioester bound with two ubiquitin like proteins, Atg8 and Atg12. Atg7 transfers each to a specific cognate E2-like enzyme, Atg3 and Atg10, and they are typically conjugated to the substrates phosphatidylethanolamine (PE) and Atg5, respectively (Fig. 1). These two conjugation systems play crucial roles in autophagy.

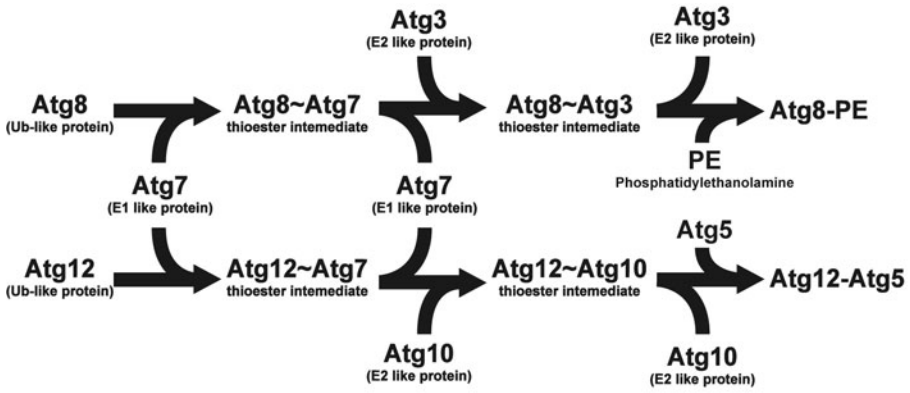

Fig.1. Schematic representation of Atg8-PE and Atg12-Atg5 conjugation

Previously, it has been reported that the C-terminal region of Atg7 is essential for Atg8-PE conjugation. In our further investigation, the initial recognition of Atg8 is predominantly mediated by the C-terminal 13 residues of Atg7, which is essential for formation of Atg7~Atg8 thioester intermediate. To identify the molecular mechanism of this recognition, we performed the NMR titration experiments and complex structure determination.

[Results]

Three C-terminal truncation mutants of Atg7 (Atg7$^{\Delta C5}$, Atg7$^{\Delta C13}$, and Atg7$^{\Delta C17}$) were prepared and subjected to *in vitro* activation and pull-down assays. Atg7$^{\Delta C5}$ was severely defective and Atg7$^{\Delta C13}$ and Atg7$^{\Delta C17}$ showed no activity for formation of Atg7~Atg8 thioester intermediates. These results

Keywords: Autophagy, complex, solution structure

are consistent with pull-down experiments showing that Atg7$^{\Delta C5}$ has reduced affinity, Atg7$^{\Delta C13}$ and Atg7$^{\Delta C17}$ have no affinity for Atg8. These data suggested that initial recognition of Atg8 is predominantly mediated by the C-terminal 13 residues of Atg7, which is essential for forming the Atg7~Atg8 thioester intermediate. To structurally elucidate the interaction of Atg7 C-terminal region with Atg8, we used NMR methods to study the interaction of Atg8 with a peptide corresponding to the residues 601-630 of Atg7 (Atg7^{C30}). Atg7^{C30} directly binds Atg8 in an *in vitro* pull-down assay. First, we titrated unlabeled Atg^{C30} into a ^{15}N-labeled sample of Atg8. Addition of AtgC30 resulted in significant shifts for many cross-peaks in [^{1}H-^{15}N] HSQC spectrum of Atg8. The residues that showed large chemical shift perturbations were clustered at on face composed of α1, α2, β2 and α3 of Atg8. Next, in order to identify the residues of Atg7^{C30} involved in the interaction with Atg8, we performed the reciprocal NMR titration experiment, titrating unlabeled Atg8 into ^{15}N-labeled Atg7^{C30} shifted significantly, especially those from the main chains of Phe^{619}, Trp^{621}, Ile^{629} and Ala^{630}.

To obtain detailed insights into the interaction, we determined the solution structure of the Atg8-Atg7^{C30} complex (Fig. 2). The overall structure of Atg8 is similar to those of free Atg8 and Atg8 in complex with the Atg8-family interacting motif (AIM) of Atg19 except for α1, which is shifted ~5 Å toward β2 compared with the Atg8-Atg19^{AIM} complex structure. A total of 3 hydrophobic pockets are visible in Atg8. Two are the W- and L-sites which are responsible for recognizing Trp and Leu residues of AIM. The third is between the relocated α1 and α2 helices.

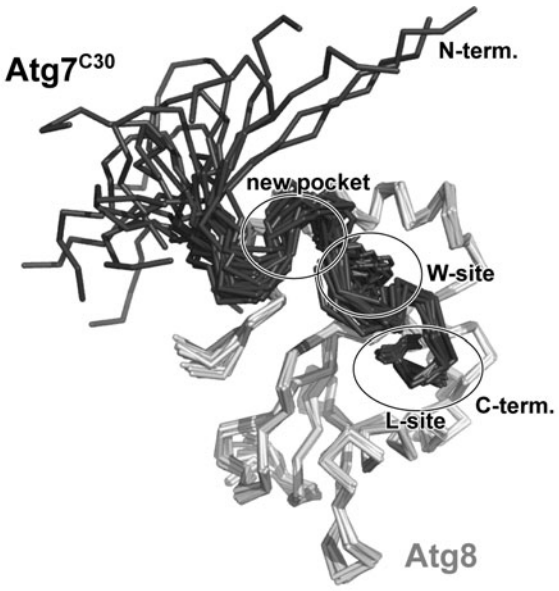

Fig. 2. NMR structure of the Atg8-Atg7^{C30} complex

Structures of the N-terminal 10 residues of Atg7^{C30} did not converge. The C-terminal 20 residues of Atg7^{C30} (residues 611-630) have a winding conformation with no secondary structure, and form extensive interactions with Atg8. The side-chain Phe^{619} is bound to the W-site of Atg8, and Ile^{629} and Ala^{630} both occupy the L-site of Atg8. These interactions are reminiscent of the Atg8-AIM interactions, although the do not form an intermolecular β-sheet commonly observed between Atg8 and AIMs. In addition, the side-chain of Val^{618} is bound to the hydrophobic pocket newly formed by α1 movement. Besides these hydrophobic interactions, ionic interactions are formed by acidic residues in the C-terminal region of Atg7^{C30} including Asp^{617}, Asp^{624}, Glu^{625} and Glu^{628}, which are surrounded by basic residues of Atg8 including Arg^{20}, Arg^{24}, Arg^{28}, Lys^{46} and Arg^{67}.

In this presentation, we will discuss the molecular mechanisms of the initial step of Atg8-PE conjugation reaction.

P-028
Y

Elucidation of the DNA-binding dynamics of the transcription factor Oct3/4 POU homeodomain

Tsuyoshi Konuma, Erisa Harada and Kenji Sugase
Bioorganic research institute, SUNTORY foundation for life sciences

Abstract

Transcription factors locate effectively to their target DNA, but the details for the dynamic search process are still largely unknown. We have investigated the DNA-binding mechanism of the POU homeodomain (POU_{HD}) of Oct3/4 using NMR. When we titrated the target DNA into POU_{HD}, almost all peaks of POU_{HD} shifted nonlinearly, indicating the existence of a binding intermediate state. To obtain structural information on the intermediate, CLEANEX-PM was measured. It is revealed that α3-helix responsible for DNA binding is partially loosened in the intermediate. These results suggest that the structural flexibility is important for nonspecific binding to DNA.

Introduction

The formation of specific protein-DNA complexes is one of crucial processes for transcriptional regulation, translation, cellular signal transduction and so on. Numerous studies have been carried out to address the question of how a protein can readily find its target site within a sea of nonspecific DNA sequences. It is generally accepted that a protein first binds nonspecifically to DNA, and then searches for a specific site according to one or a mixture of three mechanisms: sliding, jumping, and intersegment transfer. Although the dynamic DNA recognition processes should be comprised of multiple routes, in which intermediates are transiently formed, the details are largely unknown. Thus, it is essential to elucidate such intermediates to understand the DNA-binding mechanism.

The transcription factor Oct3/4, an important transcription regulator during early development in cells, has two DNA-binding domains: the specific domain (POUs) and the homeodomain. Oct3/4 is known to regulate various genes, but interestingly, POU_{HD} binding sites are not very homologous to each other whereas POU_s binding sites are strictly same. Therefore, it is supposed that the nonspecificity of POU_{HD} is important for rapid exploration of the specific DNA sequences. In this study, we have investigated the dynamics of POU_{HD} upon DNA binding using NMR.

Results and Discussions

Firstly, we titrated 16-bp DNA containing an Oct3/4 binding site (*utf*1) into [^{15}N]-POU_{HD} to characterize the conformational change and binding dynamics upon DNA binding. The concentration ratios were ranged from 0:1 (=*utf*1:POU_{HD}) to 1.2:1. The interaction was in fast exchange on the chemical shift timescale. POU_{HD} was fully saturated with DNA at 1.2:1 ratio since all POU_{HD} signals did not move at the ratio. Fig 1 shows the averaged chemical shift

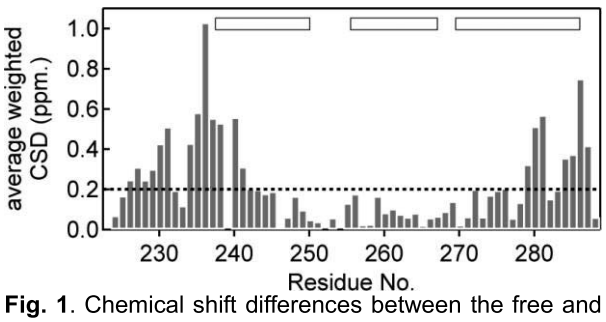

Fig. 1. Chemical shift differences between the free and *utf*1-bound states of POU_{HD}. Dashed line is the standard deviation. Open boxes represent α-helices in POU_{HD}.

Transcription factor, CLEANEX-PM, Stoichiometry analysis

differences (CSD) between the free and bound states. As the N-terminal loop and α3-helix showed large chemical shift changes, these regions undergo conformational change upon binding to *utf*1. Interestingly, several peaks in the N-terminal region, which corresponds to the nuclear localization sequence composed of many basic residues, showed two or more sets of bound peaks. This means that the N-terminal region can adopt two or more conformations. This is reasonable because this region is intrinsically disordered. In the crystal structure, the N-terminal region mainly binds to the sugar-phosphate backbone in the minor groove. The sugar-phosphate backbone has little structural difference in double stranded DNAs, therefore it is supposed that POU_{HD} binding to DNA is initiated by the nonspecific interaction between the N-terminal intrinsically disordered region and the minor groove of DNA.

During the DNA titration, almost all peaks shifted sigmoidally as shown in Fig. 2. They could not be fit to the simple two-state binding model. Therefore, a binding intermediate state should be considered to explain the titration data. Here, we constructed a new binding model using the Bloch-McConnell equation, which describes the time evolution of magnetization including the chemical exchange effect. From the fitting, we obtained kinetic parameters for POU_{HD} binding to *utf*1.

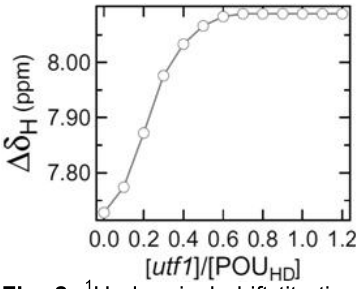

Fig. 2. ^1H chemical shift titration curve for Arg281.

Subsequently, to obtain structural information on the intermediate state, CLEANEX-PM, which determines exchange rates between amide and water protons, was applied to POU_{HD} at several concentration ratios. For Arg280 in α3-helix, no CLEANEX-PM peaks were detected in the free (0:1=*utf*1:POU_{HD}) or bound (1:1) states, meaning that the structure around Arg280 is rigid. However, CLEANEX-PM peaks of Arg280 were observed around at 0.4:1 ratio, indicating that its amide proton is water-exposed. This is quite curious because α3-helix is partially loosened when there is an excess of POU_{HD} whereas it is rigid in the free and the bound states. Since the specific binding site on *utf*1 is saturated with POU_{HD} at 0.4:1 ratio, a nonspecific complex that we assume as the intermediate is prone to be formed. Taking a careful look at the crystal structure, the guanidino group of Arg280 is located at the vicinity of a phosphate group in *utf*1, but it forms hydrogen bonds with the carboxyl group of Glu245 in α1-helix (Fig. 3). Therefore, it is suggested that the intermediate state lacks the native hydrogen bond between Arg280 and Glu245, and Arg280 interacts with phosphate groups in DNA to accomplish the nonspecific binding.

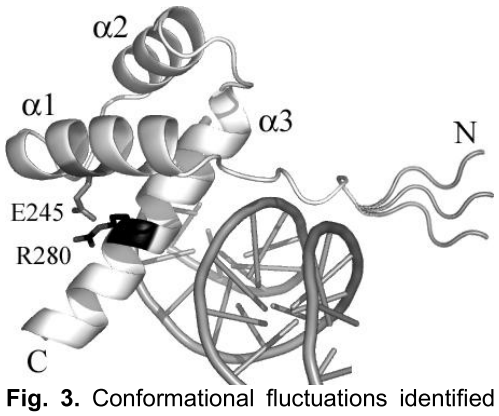

Fig. 3. Conformational fluctuations identified from the titration and CLEANEX-PM experiments. The N-terminal region adopts multiple conformations in the bound state, and α3-helix around Arg280 (black) is partially loosened in the intermediate.

In conclusion, we elucidated the dynamics of POU_{HD} upon binding to *utf*1, the NMR analysis presented here showed that the structural flexibility of POU_{HD} is important for nonspecific binding to DNA.

P-029 Structure and dynamics of yeast calmodulin

Kenji Ogura[1], Hideyasu Okamura[2], Hiroyuki Kumeta[1], Michio Yazawa[3], and Fuyuhiko Inagaki[1]
[1]Faculty of Advanced Life Science, Hokkaido University,
[2]Institute of Advanced Energy, Kyoto University, and
[3]Graduate School of Science, Hokkaido University

ABSTRACT

We determined the solution structures of yeast calmodulin (yCaM) in Ca^{2+}-bound state and the target peptide-bound state. In contrast to vertebrate CaM, the Ca^{2+}-bound yCaM showed a compact globular structure consisting of the EF1, 2 and 3 motifs excluding the disordered EF4 motif, while the target-bound yCaM closely resembled vertebrate CaM-peptide complex. The relaxation dispersion profiles of the Ca^{2+}-bound yCaM showed a conformational exchange in a boundary surface between the N-terminal domain and the EF3 motif. The results suggested the target recognition of yCaM is regulated by the open-close transition of the EF3 motif.

INTRODUCTION

Calmodulin (CaM) is a Ca^{2+} signaling protein which consists of two globular domains each comprised of two EF-hand motifs and a flexible linker. A pair of Ca^{2+} binding sites is located on each globular domain. The EF-hand motifs are referred to as EF1, EF2, EF3, and EF4, from the N-terminus, and CaM can bind a total of four Ca^{2+} ions. Many structural studies by X-ray crystallography and NMR have revealed a Ca^{2+}-dependent activation process of CaM. Apo CaM and Ca^{2+}-bound CaM have structurally isolated N- and C-terminal globular domains which tumble in an independent manner. CaM is a highly conserved protein ubiquitously expressed in eukaryotic cells. The amino acid sequences of the canonical CaM isoforms are nearly identical with sequence identities of more than 90%.

The amino acid sequence of yeast CaM (yCaM), however, shares only ca 60% identity with canonical CaM. This sequence difference provides yCaM with unique Ca^{2+}-binding properties. Earlier works have shown that due to the substitution of highly conserved Asp and Glu residues in EF4 of yCaM, EF4 lacks the Ca^{2+}-binding ability and, hence, yCaM can bind only three Ca^{2+} ions per molecule. Moreover, earlier studies have also shown that the N- and C-terminal domains of yCaM interact with each other in the Ca^{2+}-bound state, which is not observed in the canonical CaM isoforms. The NMR solution structure of yCaM in apo form is very similar to those of the vertebrate CaM isoforms (1), and no interaction between the N- and C-terminal domains is observed.

Here, we determined the structures of yCaM both for the Ca^{2+}-bound and target peptide-bound states using NMR spectroscopy. As the target peptide, we used a calcineurin A1 subunit-derived 24 amino acid-containing peptide, denoted as the CNA1-peptide. Moreover, to analyze a conformational exchange of the Ca^{2+}-bound yCaM, the ^{15}N relaxation dispersion data were measured on different magnetic fields.

---

yeast, calmodulin, relaxation dispersion

MATERIALS AND METHODS

A recombinant yeast calmodulin (denoted as yCaM; 146 amino acids) and an EF4 Ca^{2+}-binding site-deleted yCaM mutant, corresponding to the EF1-3 regions of yCaM (referred to as yCaM (1-120)), with a C-terminal hexahistidine-tag were cloned into the pET22b expression vector. A single-chain chimeric protein mimicking a complex of intact yCaM and the target-peptide derived from yeast calcineurin A1 subunit (referred to as CNA1-peptide; 24 amino acids) was cloned into a pGEX6P expression vector. The chimeric protein (referred as yCaM-CNA1) consisted of a total of 175 residues (146 yCaM residues, a five-residue linker GSSTG, and 24 CNA1-peptide residues).

All the protein samples were overexpressed in *E.coli* strain BL21 (DE3) transformed by the expression vectors. Uniformly isotope labeled samples were expressed in medium containing $^{15}NH_4Cl$ and [^{13}C] glucose. The intact yCaM and yCaM (1-120) were purified using a Ni-NTA affinity resin. The GST-fused yCaM-CNA1 was purified using a glutathione-Sepharose 4B column, and GST was excised from the yCaM-CNA1 with PreScission protease. The samples were purified using a Superdex75 gel filtration column.

All the NMR measurements were carried out at 25 °C and the samples were prepared in 20 mM MES-NaOH buffer (pH 6.5), 5 mM $CaCl_2$ and 150 mM NaCl. Two- and three-dimensional NMR experiments were performed on Varian Inova spectrometers operating at 800 or 600 MHz. ^{1}H, ^{13}C and ^{15}N resonance assignments were carried out using the standard set of spectra. The heteronuclear $\{^{1}H\}$-^{15}N NOE experiment was performed using ^{15}N-labeled intact yCaM in the Ca^{2+}-bound state. The ^{15}N relaxation dispersion data of the Ca^{2+}-bound yCaM(1-120) were acquired using an rcCPMG pulse sequence (2).

The structures of the Ca^{2+}-bound yCaM(1-120) and Ca^{2+}-bound yCaM-CNA1 were calculated using the Cyana software with interproton distances derived from ^{13}C-edited and ^{15}N-edited NOESY spectra using a 75 ms mixing time and dihedral angle restraints predicted by Talos software.

To analyze the relaxation dispersion data of Ca^{2+}-bound yCaM(1-120), initially, data for 19 residues (out of data available for 114 residues) were selected based on their large ^{15}N chemical shift differences. Then the data were retained on the basis of their residual χ_2 values after trial fits of their global kinetic parameters with their residue-specific $\Delta\omega$ values fixed. Next, to determine the global kinetic parameters, a cycle consisting of residue-specific fits for $\Delta\omega$ and R_{20}, followed by a global fit for the kinetic parameters was repeated until the total χ_2 value was reduced in size. Finally, for each of the 114 residues, their $\Delta\omega$ and R_{20} values were fit with the calculated kinetic parameters fixed. Errors associated with the parameters used in the fits were estimated by Monte Carlo simulations.

RESULTS AND DISCUSSION

The sequential backbone resonance assignments of intact Ca^{2+}-bound yCaM were obtained using a combination of triple-resonance spectra. The $\{^{1}H\}$-^{15}N heteronuclear NOE data of the intact Ca^{2+}-bound yCaM indicated that residues 116-146 showed weak (< 0.6) NOE intensities that were interpreted to be highly flexible. Therefore, the EF4-deletion mutant of yCaM, comprising of the EF1-3 regions (referred to yCaM (1-120)), was prepared and analyzed by NMR spectroscopy.

The sequential backbone resonance assignments of Ca^{2+}-bound yCaM (1-120) were also completed. The solution structure of Ca^{2+}-bound yCaM (1-120) was calculated. The ribbon model of the lowest energy structure is shown in Fig. 1. As expected, Ca^{2+}-bound yCaM (1-120) formed a single compact domain consisting of six α-helices in agreement with those of apo yCaM. As the individual partner helices in each EF-hand region take a perpendicular orientation, all the EF-hand motifs in Ca^{2+}-bound yCaM (1-120) are classified into a so-called 'open' conformation. In canonical CaM, the N- and C-terminal domains show no interaction with each other in the Ca^{2+}-bound form. Intriguingly, yCaM (1-120) presented a collapsed structure showing a close interaction between the N-terminal domain (EF1 and 2) and the EF3 region of the C-terminal domain.

A fit of ^{15}N relaxation dispersion data with a two-site model yielded the global k_{ex} (rate constant of chemical exchange) value of 262 s^{-1} and p_A (equilibium population of site A) of 0.93 for the Ca^{2+}-bound yCaM(1-120). Fig.2 shows the Δω (chemical shift difference between two sites) values as functions of amino acid sequence. Large values of Δω for residues in EF3 region indicate conformational change of the EF3 region. Mapping of Δω values onto the solution structure of Ca^{2+}-bound yCaM(1-120) (Fig. 3) shows that the residues in large Δω are located at the interacting surface between the N-terminal domain (residues 1-79, EF1 and EF2) and the EF3 region (residues 80-120). This result suggests that the ^{15}N relaxation dispersion profiles of Ca^{2+}-bound yCaM(1-120) are derived from an open-close conformational exchange of the EF3 region. The presence of the conformational exchange is in reasonable agreement with functions of the target-recognition of yCaM.

The solution structure of yCaM-CNA1 was calculated based on the resonance assignment, inter-proton distances, and dihedral angle restraints. The ribbon model of the lowest energy structure is shown in Fig. 4. The CNA1-peptide adopts an α-helical conformation around which, the N- and C-terminal domains of yCaM wrap to form a largely globular complex similar to other structures in the typical CaM-peptide complexes. Interestingly, the EF4 region, which forms a disordered conformation in the absence of the target peptide, refolds itself to be involved in target recognition, forming a perpendicular orientation (*i.e.*, an open conformation) of a pair of helices. Although the pair of helices in the EF4 region of yCaM-CNA1 shows a perpendicular orientation, Ca^{2+} was not bound to the EF4 region of yCaM-CNA1. Detail of hydrophobic contacts between the anchor residues of CNA1 and yCaM mean that the yCaM-CNA1 complex is classified into the 1-5-8-14 group.

The N-terminal domains (EF1 and EF2) of yCaM(1-120) and yCaM-CNA1 are quite similar to each other, where the structural rmsd of the main chain atoms of residues 10-75 is 1.5 Å. The hydrophobic patches on the N-terminal domain of yCaM are masked either by the EF3 region or by the target peptide. In addition, yCaM recognizes the target peptide via the N- and C-terminal domains in a similar manner to the canonical CaM isoforms. Since the canonical CaM isoforms in the Ca^{2+}-bound state show no interaction between the N- and C-terminal domains, it is intriguing to consider the reason why yCaM forms such a collapsed structure. Probably, the collapsed form in the Ca^{2+}-bound yCaM is due to the loss of Ca^{2+}-binding ability in EF4. It is widely accepted that a pair of EF-hand motifs in the canonical CaM isoforms are stabilized by each other upon binding to Ca^{2+}. In yCaM, because EF4 is unable to bind Ca^{2+}, EF3 cannot stabilize the Ca^{2+}-bound form of the C-terminal domain. Once Ca^{2+} ions are bound to the N-terminal domain of yCaM (EF1 and 2), the structural transition occurs to expose the hydrophobic patches, which are stabilized by interaction

with the hydrophobic surface of EF3. Thus, yCAM is capable of forming the compact, collapsed structure in the Ca^{2+}-bound state. As EF4 loses its structural partner (EF3), it turns into a disordered and flexible structure.

REFERENCES

(1) Ishida et al., Biochemistry 41, 15536 (2002).
(2) Hansen et al., J. Phys. Chem. B 112, 5898(2008).

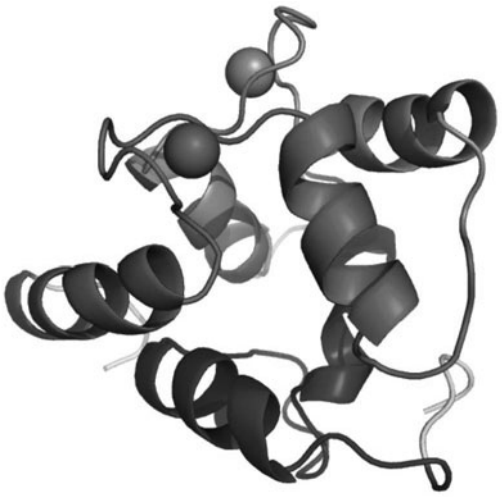

Fig. 1 Ribbon diagram of the solution structure of Ca^{2+}-bound yCaM(1-120).

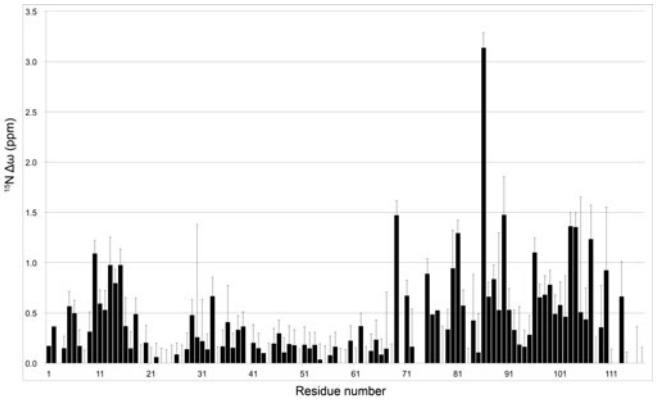

Fig. 2 ^{15}N chemical shift difference of Ca^{2+}-bound yCaM(1-120) between the major and minor states.

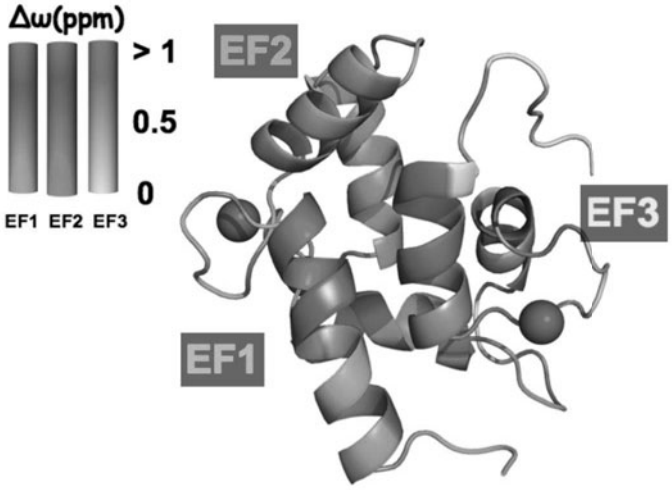

Fig. 3 Ca^{2+}-bound yCaM(1-120) colored according to the ^{15}N chemical shift difference between the major and minor states.

Fig. 4 Ribbon diagram of the solution structure of Ca^{2+}-bound yCaM-CNA1.

P-030 Incorporation of an additional hydrogen bond in the active site of *Hydrogenobacter thermophilus* cytochrome c_{552} by means of protein engineering and its structural and functional consequences

Akihiro Sugimoto, Shin-ichi Mikami, Naoya Shinohara, Hulin Tai, and Yasuhiko Yamamoto
Department of Chemistry, University of Tsukuba

We have succeeded in introducing a hydrogen bond in the active site of *Hydrogenobacter thermophilus* cytochrome c_{552} through an amino acid substitution, i.e., V53N mutation. Structural and functional consequences of the hydrogen bond have been characterized in order to elucidate the structure-function relationship of the protein. The study demonstrated that its formation results in structural alteration of a peptide loop in close proximity to heme, which in turn allows the access of water molecules to the heme active site. The effect of the solvent reorientation on the redox property of the protein was clearly manifested in the mutation induced-change of the entropic term of the redox potential.

INTRODUCTION

Hydrogenobacter thermophilus cytochrome c_{552} (HT (Fig. 1 left)) is an electron transfer protein, composed of 80 amino acid residues and heme as a prosthetic group[1]. The heme Fe is coordinated to a His and a Met as axial ligands. In this study, we attempted to alter the structure of the loop through a V53N and V53Q mutation in order to elucidate the relationship between the redox property of the protein and the loop structure. Val53 is also located in the functionally relevant loop, and its amide NH hydrogen atom forms a hydrogen bond with the heme 13-propionic acid side chain (Fig. 1 right)[2]. In addition to this hydrogen bond, the heme 13- and 17-propionic acid side chains are anchored to the protein moiety through an elaborated hydrogen bond network[3]. We expected that the introduced side chain amide groups through the mutations participate in this hydrogen bond network.

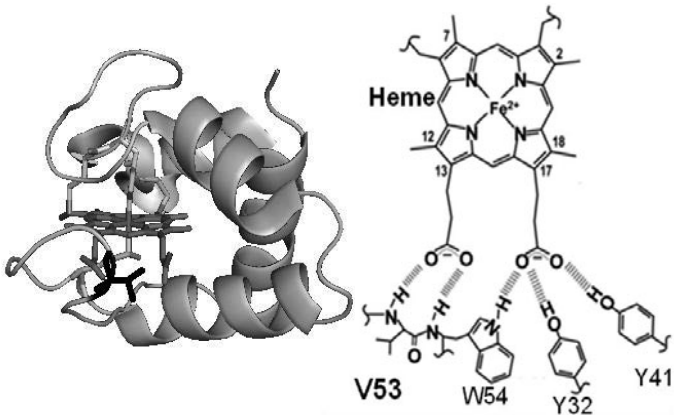

Fig. 1. Structure of *Hydrogenobacter thermophilus* cytochrome c_{552}.Polypeptide chain is represented by ribbon model, and heme, Cys10, Cys13, His14 and Met59 by stick model(left)(PDB:1YNR). Hydrogen bonds between the residues and heme(right).

RESULTS AND DISCUSSION

The resolved ^{1}H NMR signals of the reduced forms of the three proteins considered here were similar to each other(Fig. 2). One of the characteristics of the V53N mutant spectrum is the appearance of an additional exchangeable proton signal at 9.88 ppm, which is likely to arise

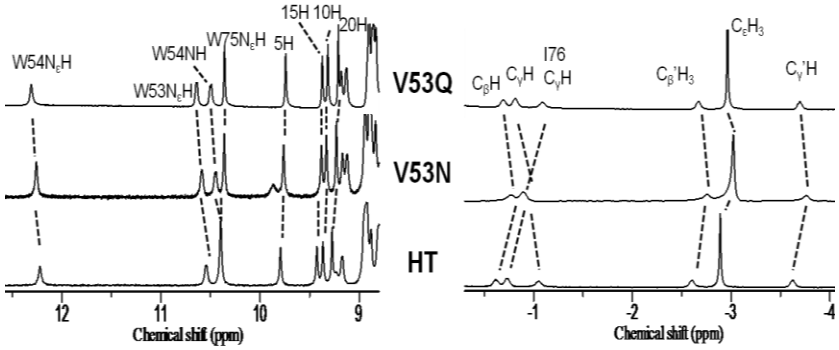

Fig. 2. Resolved ^{1}H NMR signals of the reduced V53N(middle) and V53Q(top) mutants and the wild-type HT(bottom) at pH 7.0 and 25 ˚C.

Keywords: paramagnetic shift, cytochrome *c*, hydrogen bond

from the Asn53 side chain NH proton. Structural similarity among the three proteins has been confirmed through a comparison of their HSQC spectra (Fig. 3). The signals were observed at 9.88 and 7.15 ppm, respectively Asn53 $N_{\delta}H$ and $N_{\delta'}H$ protons. The downfield shift of the $N_{\delta}H$ proton signal indicated that this proton participates in a hydrogen bond, and the relatively large shift difference, i.e., 2.73 ppm were observed between the signals. On the other hand, such an additional NH proton signal was not observed in the downfield-shifted region of the spectrum of the V53Q mutant, suggesting that the Gln53 side chain does not participate in a hydrogen bond.

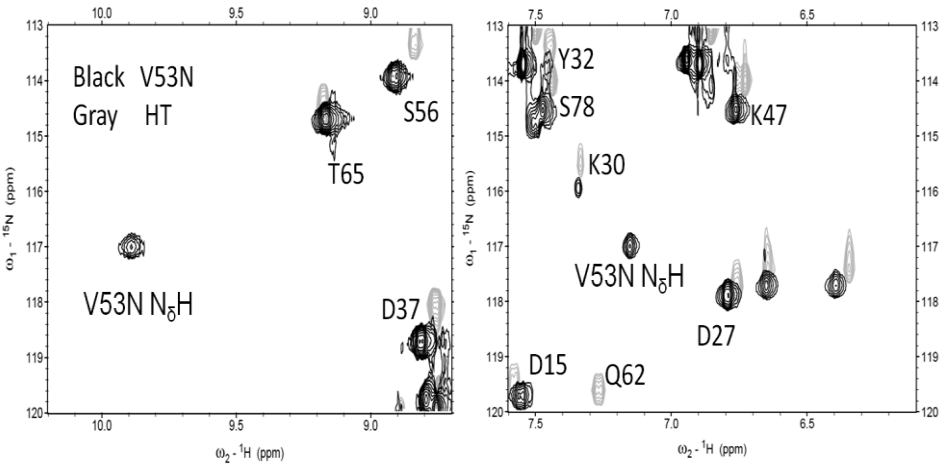

Fig. 3. Overlay of positions of $^1H/^{15}N$ HSQC spectra of the reduced forms of the V53N mutant (black) and the wild-type HT(gray) at pH 6.0 and 25 ˚C.

The denaturation temperature (T_m), the E_m value, and the enthalpic (ΔH) and entropic (ΔS) contributions to the E_m value of the proteins are summarized in Table 1. The plots of the E_m values against temperature for the proteins could be fitted by two straight lines with a transition temperature (T_c) of ~35 ºC, and hence two sets of the ΔH and ΔS values in the temperature ranges of $\leqq T_c$ and $\geqq T_c$ were determined for the proteins. The V53N and V53Q mutations resulted in lowering the T_m value by ~2 - ~8 ºC. Hence the hydrogen bond formed by the Asn53 side chain NH in the V53N mutant did not contribute to an increase in the protein stability, but even lower the thermostability. The significant decrease in the $-T\Delta S$ value due to the V53N mutation is attributed to an increase in the contribution of the redox-dependent solvent reorganization. The loop structure is likely to be affected by the hydrogen bond formed by the Asn53 side chain NH, and the access of water molecules to the heme active site appeared to be enhanced by the mutation-induced structure change. The decrease in the T_m value by the V53Q mutation could be attributed to destabilization of the heme hydrophobic environment by the mutation. The slight decrease in the $-T\Delta S$ value due to the V53Q mutation is attributed to slightly increased contribution of the redox-dependent solvent reorganization.

Table 1. Thermodynamic parameters for reduction and thermal unfolding of the proteins at pH 6.0 and 25 ºC.

Protein	T_m(°C)				ΔH(KJ mol^{-1})		$-T\Delta S$ (KJ mol^{-1})	
	oxidized	reduced	ΔT_m	E_m (mV)	low	high	low	high
HT	109.8	129.7	19.9	245.0	−32.2	−37.5	8.5	13.6
V53N	104.4	127.7	23.3	231.6	−25.6	−30.0	3.2	7.6
V53Q	102.0	122.0	20.0	240.1	−29.8	−35.6	6.7	12.2

Denaturation temperature(T_m) determined through analysis of the temperature dependence of the CD ellipticity at 222 nm and pH 7.0. The experimental error was ± 0.2 ºC.
Redox potential determined at pH 6.0 and 25 ºC. The experimental error was ± 2 mV.
Entropic and enthalpic contributions to the E_m value at pH 6.0. experimental errors for ΔH and $T\Delta S$ of the proteins were ± 2 kJ mol^{-1} and ± 3 kJ mol^{-1}, respectively.

REFERENCES

[1]Y. Sanbongi *et al.*, *J. BACTERIOL,* 1989, 171, 64-69.

[2]H. Tai *et al., Biochemistry*, 2011, 50, 3161-3169.

[3]H. Tai *et al.*, *Biochemistry*, 2010, 49, 42-48.

P-031 NMR studies on the histone H2A/H2B hetero-dimer and histone chaperones, NAP1 and NAP2

Yoshihito Moriwaki[1], Mitsuru Okuwaki[2], Kyosuke Nagata[2], Msahiko Sato[1], Aritaka Nagadoi[1] and Yoshifumi Nishimura[1]
[1]Grad. Sch. of Supermol. Biol, Yokohama City Univ.
[2]Grad. Sch. of Comprehensive Human Sciences, Univ. of Tsukuba

ABSTRACT

A nucleosome core is comprised of 147 bp of DNA and a histone octamer, consisting of two copies of four kinds of histones, H2A, H2B, H3 and H4. Dissociation and association of histones in the nucleosome core occur dynamically in the region where the gene expression is active. It is indispensable to analyze each of dissociated parts. In addition, histone chaperones are closely related to dissociation and association of histones. Here, we determine the structure of the H2A/H2B hetero-dimer and the interaction mode of H2A/H2B with histone chaperones, NAP1 and NAP2 by NMR.

The structual analysis of H2A/H2B hetero-dimer

In eukaryotic cells, DNA is stably stored in a highly ordered structure, chromatin. Its fundamental repeating structural unit is a nucleosome core, which is comprised of 147 bp of DNA and a histone octamer, consisting of two copies of four kinds of histones, H2A, H2B, H3 and H4. Dissociation and association of histones in the nucleosome core occur dynamically in the region where the gene expression is active. Although the crystal structure of the nucleosome core particle has already been determined, the structure of isolated H2A/H2B hetero-dimer remains unknown. It is crucial to analyze a dynamic structure of the H2A/H2B hetero-dimer for understanding the chromatin reorganization. We analyze the structure of the H2A/H2B hetero-dimer.

Fig.1 shows the ^{1}H-^{15}N TROSY-HSQC spectora of the ^{2}H, ^{13}C, ^{15}N labeled H2A/^{2}H,^{13}C, ^{15}N labeled H2B hetero-dimer. We could assign backbone chemical shifts (HN, N, Cα, Cβ, C') of H2A and H2B individually, and derived the secondary structure from the chemical shift indexes (fig.2). We found that the N-terminal and C-terminal regions of H2A in isolated H2A/H2B hetero-dimer take no secondary structure, in contrast that these regions hold α-helixes in nucleosome core particle.

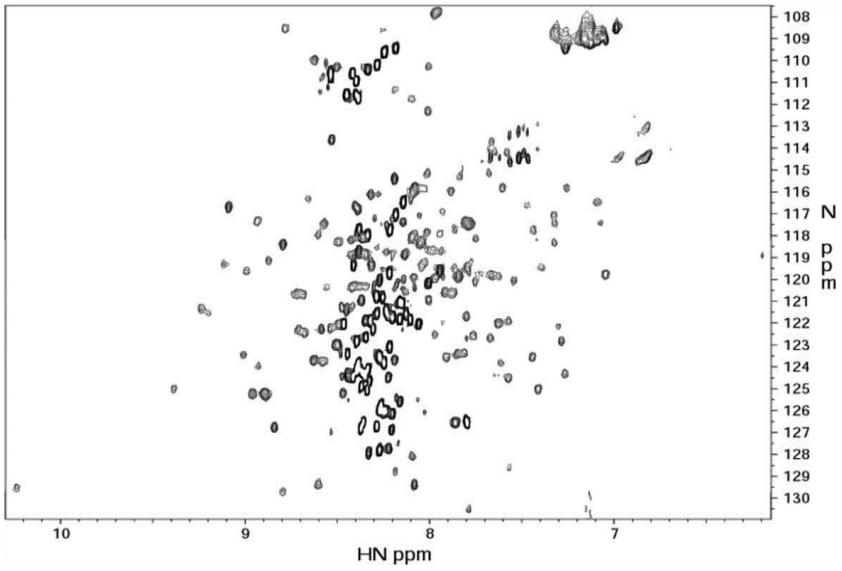

Fig.1 ^{1}H-^{15}N TROSY-HSQC spectra of he ^{2}H, ^{13}C, ^{15}N labeled H2A/^{2}H,^{13}C, ^{15}N labeled H2B hetero-dimer.

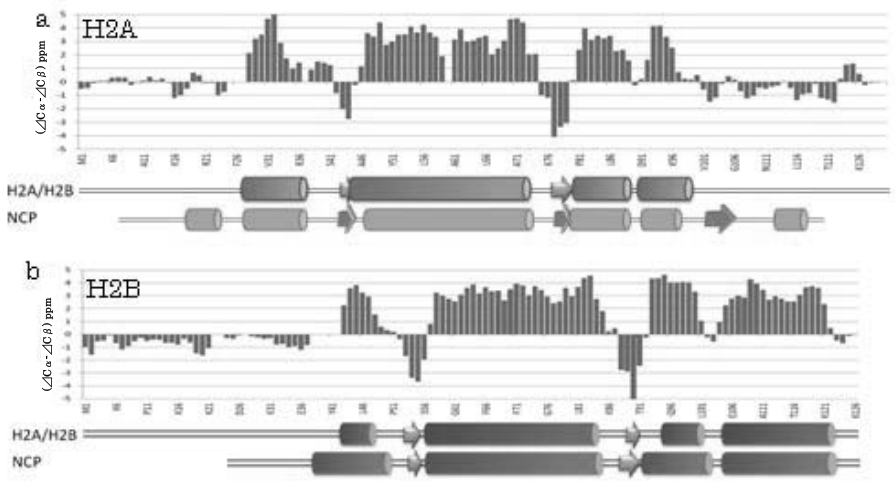

Fig.2
The secondary structures of H2A (a) and H2B (b) in isolated H2A/H2B hetero-dimer derived from the chemical shift indexes. Each secondary structures in nucleosome core particle (NCP) were also shown.

Interaction of the H2A/H2B hetero-dimer with histone chaperones

The assembly of nucleosomes is considered to occur by a 2-step process. At first, a tetramer of H3 and H4 is deposited onto DNA, and then the nucleosome core is completely terminated by the addition of two hetero-dimers of H2A/H2B. Disassembly of nucleosome core advances in the reverse process. Histone chaperones are necessary for dissociation and association of the nucleosome core under physiological conditions. Nucleosome assembly protein 1 (NAP1) is one of histone chaperones which interacts with H2A/H2B hetero-dimers. The central region of NAP1, the dimerization domain, is essential for both histone binding and nucreosome assembly. The C-terminal acidic region is required for transient removal of H2A/H2B hetero-dimers. Nucleosome assembly protein 2 (NAP2) is the homolog of NAP1. The C-terminal rehion of NAP2 is nine residue shorter than that of NAP1. We demonstrated that the interaction of the H2A/H2B hetero-dimer with the C-terminal deletion mutant is weaker than that with the wild-tipe NAP1. In addition only C-terminal acidic reasions of NAP1 and NAP2 interacts with the H2A/H2B hetero-dimer. Here, we clarify the mechanism of the interaction between C-terminal acidic reasions of NAP1 and NAP2 (NAP1C and NAP2C respectively) and the H2A/H2B hetero-dimer by solution NMR.

We observed ^{1}H-^{15}N TROSY-HSQC spectral changes of ^{2}H, ^{13}C, ^{15}N labeled H2A/^{2}H labeled H2B and ^{2}H labeled H2A/^{2}H,^{13}C, ^{15}N labeled H2B by adding nonlabeled NAP2C. And we identified the binding surface on the H2A/H2B hetero-dimer (Fig.3). Also we measured ^{1}H-^{15}N TROSY-HSQC spectra of ^{15}N labeled NAP2C with and without nonlabeled H2A/nonlabeled H2B, and identified residues of NAP2C which interact with H2A/H2B.

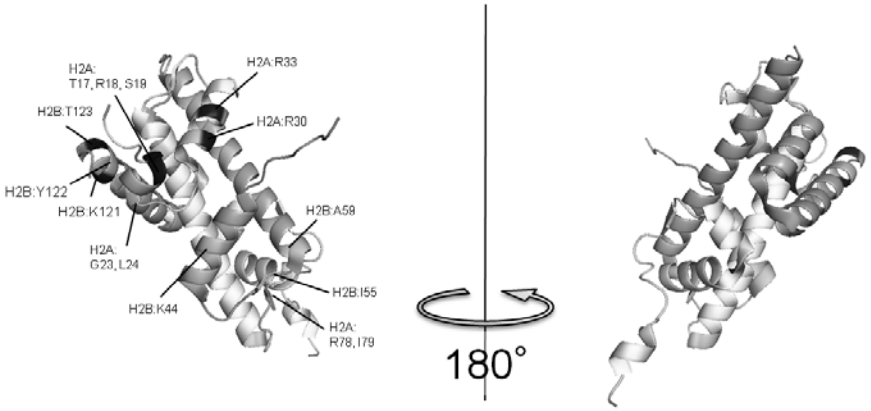

Fig.3
The H2A/H2B hetero-dimer from the crystal structure of the nucleosome core (PDB 2CV5, Tsunaka et al.). Residues whose chemical shifts changed more than 0.2 ppm by adding NAP2C are shown in black.

H2A/H2B, NAP1, NAP2

P-032 NMR analysis of an anti-carbohydrate antibody single-chain Fv fragment toward elucidation of the multivalent recognition mechanism

Ganesh P. Subedi[a,b], Tadashi Satoh[a†], Shinya Hanashima[a], Akemi Ikeda[a], Hiroshi Nakada[c], Reiko Sato[d], Mamoru Mizuno[d], Noriyuki Yuasa[e], Yoko Fujita-Yamaguchi[e], Yoshiki Yamaguchi[a,b]

[a]Structural Glycobiology Team, RIKEN, ASI
[b]Department of Bioinformatics, Tokyo Medical and Dental University
[c]Faculty of Life Sciences, Kyoto Sangyo University,
[d]Laboratory of Glyco-organic Chemistry, The Noguchi Institute
[e]Department of Applied Biochemistry, Tokai University School of Engineering
[†]Present address: Graduate School of Pharmaceutical Sciences, Nagoya City University

ABSTRACT

MLS128 antibody selectively recognizes cancer-related Tn-antigens with consecutive three GalNAc-Thr (Tn3) units. To elucidate multivalent recognition mechanisms behind the event, we prepared a corresponding single-chain Fv fragment (scFv) and analyzed by NMR. The scFv was efficiently overproduced using a novel pCold-PDI vector in *E. coli* Origami strain. NMR and ITC analyses revealed that scFv retains full binding activity towards synthetic glycopeptides having Tn3 unit. We will discuss their molecular basis on the multivalent GalNAc-Thr recognition mechanism.

Introduction

Tn antigens are aberrantly overexpressed in adenocarcinomas. These glycopeptide antigens can be potentially recognized by antibody and efficient antigen-antibody interaction can help in the development of specific biomarkers or therapeutic agents against cancer. MLS128 is one such anti-carbohydrate antibody which specifically recognizes Tn antigen consisting of both the two and three consecutively arranged GalNAc-*O*-Ser/Thr at cancerous cell surface and has been shown to inhibit colon and breast cancer cells growth possibly by down-regulation of epidermal growth factor receptor and insulin like growth factor 1 receptor (1). To elucidate the details of multivalent recognition mechanism behind this event, we prepared a corresponding single-chain Fv fragment (scFv) of MLS128 antibody as a soluble form using a novel pCold-PDI vector in Origami *E.coli* strain and analyzed by NMR (2).

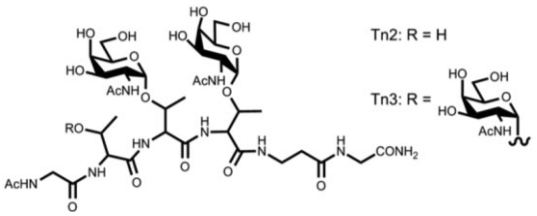

Figure 1. Chemical structure of Tn peptides used in this study. GalNAc residues are consecutively attached to threonine residues at positions 2 and 3 for Tn2 and at positions 2, 3 and 4 for Tn3 peptides.

Production of MLS128-scFv

Large quantity of sample amount is often required for structural studies. We achieved high yield production of two disulfide bond containing MLS128 scFv by using novel system containing human protein disulfide isomerase as a fusion tag in pCold vector (3) at low temperature. Using this system MLS128 scFv was successfully expressed as a soluble form in *E.coli* cytoplasm and purified in milligram order for

NMR analysis towards structural elucidation.

Biophysical nature of MLS128 scFv

The correct folding and well characterized β sheet structure of recombinant MLS128 scFv was indicated by 1D ^{1}H-NMR spectrum. For the atomic level analyses of the binding event, NMR experiments using stable-isotopes labeled scFv were performed with the ligand glycopeptides (Tn2 and Tn3) (Figure 1).

Several NMR signals derived from scFv in well separated 2D ^{1}H-^{15}N HSQC (Figure 2) were perturbed upon an addition of ligands, which clearly indicated that the peptide ligands (Tn2 and Tn3) bind to the specific binding sites. Further, isothermal titration calorimetry (ITC) revealed that scFv retains binding activity towards synthetic glycopeptides having Tn2 (K_a = 1.3 × 10^3 M^{-1}) and Tn3 units (K_a = 5.8 × 10^3 M^{-1}). For the NMR signals assignment, a series of selectively labeled samples were prepared. In the absence of Tn3 peptide in selectively Trp-labeled sample, one of the Trp residues shows two peaks presumably due to its dynamic equilibrium with two conformations which gets stabilized in the presence of Tn3 peptide (Figure 3)

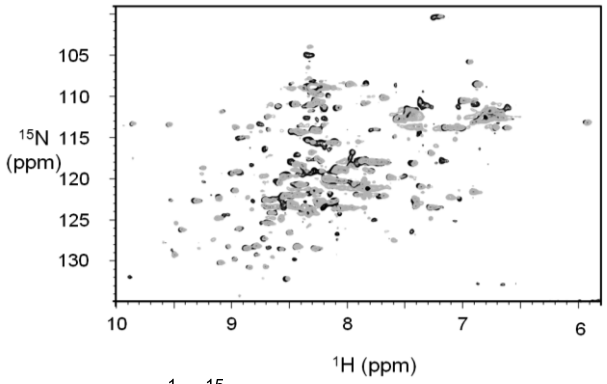

Figure 2. 2D ^{1}H-^{15}N HSQC spectra of uniformly ^{15}N-labeled MLS128-scFv (0.45 mM) in the presence (gray) and absence (black) of an equimolar amount of Tn3 peptide.

Conclusion

Well-separated signals in 1D ^{1}H NMR and 2D ^{1}H-^{15}N HSQC spectra indicate that recombinant MLS128-scFv protein attains its native conformation. Chemical shift change as well as peak broadening of specific amino acid residues reveals Tn2/Tn3 binding with MLS128 scFv. Dynamically equilibrated tryptophan residue in two conformations becomes stabilized upon binding to the peptide. Further NMR investigations are ongoing at present to reveal the multivalent binding from the dynamical aspect.

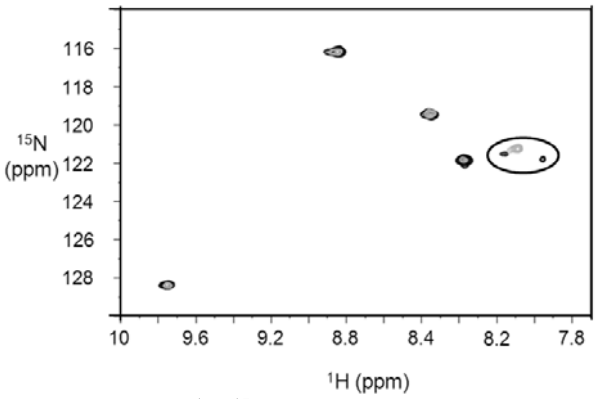

Figure 3. 2D ^{1}H-^{15}N HSQC spectra of ^{15}N-Trp-labeled MLS128-scFv in the presence (gray) and absence (black) of Tn3 peptide. The residue showing two peaks is encircled.

References

1. Morita, N., Yajima, Y., Asanuma, H., Nakada, H., and Fujita-Yamaguchi, Y. (2009), *Biosci. Trends* 3, 32-37.

2. Subedi, G.P., Satoh, T., Hanashima, S., Ikeda, A., Nakada, H., Sato, R. Mizuno, M., Yuasa, N., Fujita-Yamaguchi, Y., Yamaguchi, Y., submitted.

3. Qing, G., Ma, L. C., Khorchid, A., Swapna, G. V., Mal, T. K., Takayama, M. M., Xia, B., Phadtare, S., Ke, H., Acton, T., Montelione, G. T., Ikura, M., and Inouye, M. (2004), *Nat. Biotechnol. 22*, 877-882.

Key words: anti-carbohydrate antibody, single-chain antibody fragment, Tn-antigen

P-033 Title NMR analyses of membrane-proximal C-terminal tail of chemokine receptor CCR2 bound to a cytosolic protein FROUNT and membrane

Kaori Esaki[1], Sosuke Yoshinaga[1], Takashi Saitoh[2], Toshiyuki Kohno[3], Ichio Shimada[4], Yuya Terashima[5,6], Etsuko Toda[5], Kouji Matsushima[5] and Hiroaki Terasawa[1]

[1]Grad. Sch. Pharm. Sci., Kumamoto Univ., [2]Med. Inst. Bioreg. Kyushu Univ., [3]Mitsubishi Kagaku Inst., Life Sciences, [4]Grad. Sch. Pharm. Sci., Univ. Tokyo, [5]Grad. Sch. Med., Univ. Tokyo, [6]ECI, Inc.

ABSTRACT

The chemokine receptors CCR2 and CCR5 regulate leukocyte migration. Interaction between the membrane-proximal C-terminal region (Pro-C) of the receptors and a cytosolic protein FROUNT is necessary for chemokine signaling.

NMR analyses showed that CCR2 Pro-C is able to fold into an α-helix after interacting with either FROUNT or cell membrane, and the hydrophobic surface of CCR2 Pro-C is important for both interactions. NMR cross saturation (CS) experiments and surface plasmon resonance (SPR) analyses indicated that the affinity of CCR2 Pro-C to FROUNT is higher than that of CCR2 Pro-C to cell membrane. Based on these data we hypothesized that a ligand-induced conformational change of CCR2 is required for FROUNT binding and downstream signaling.

[Introduction]

Chemokine receptors play a pivotal role in immune cell recruitment to inflammation sites, in response to chemokine gradients (chemotaxis). This innate immune response is required for host defense, although when it becomes uncontrolled, it leads to inflammatory disease. Approximately 20 plasma membrane receptors have been characterized as members of the chemokine receptor family, and all of them are G protein-coupled receptors (GPCRs). Mutational analyses revealed that the Pro-C region of chemokine receptors plays an important role in chemotaxis. However, very little is known about the molecular mechanisms associated with the Pro-C region.

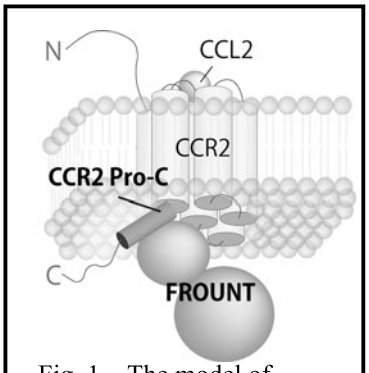

Fig. 1 The model of CCR2—FROUNT complex.

In the case of the chemokine receptors CCR2 and CCR5, the truncation of the Pro-C region impairs the chemokine signalling without the loss of cell surface localization. We previously determined, using a yeast two hybrid system, that FROUNT directly binds to chemokine-bound forms of CCR2 and CCR5, and mediates directional cell migration (Fig. 1). In this study we used NMR and SPR to elucidate the mechanism of chemokine signaling, focusing on the interaction between FROUNT and CCR2 Pro-C.

FROUNT, Chemokine receptor, GPCR

[Results and discussion]

To determine the solution structure of a CCR2 Pro-C bound to FROUNT, we investigated the transferred nuclear Overhauser effects (TRNOEs) of CCR2 Pro-C peptide in the presence of FROUNT. Although the CCR2 Pro-C peptide itself is unable to fold, upon binding to FROUNT it is able to fold into a right-handed helical conformation that creates an amphipathic surface. Using transferred cross saturation (TCS) experiments, we revealed that FROUNT-binding residues are on the hydrophobic surface of CCR2 Pro-C.

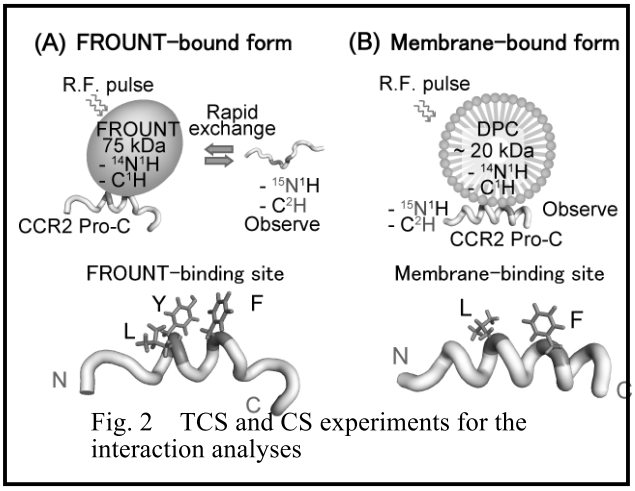

Fig. 2 TCS and CS experiments for the interaction analyses

Because the CCR2 Pro-C region of the receptor is located just after the transmembrane domain, it is expected to interact with the plasma membrane. The structure of CCR2 Pro-C was investigated by NMR in the presence of dodecylphosphocholine (DPC) micelles, which are thought to simulate the membrane environment. The data revealed that CCR2 Pro-C can fold into an amphipathic α-helix after interacting with the micelles. These results suggested that CCR2 Pro-C can fold into an α-helix following interaction with the plasma membrane. Using NMR CS experiments, it was shown that the membrane-binding residues are on the hydrophobic surface of CCR2 Pro-C and overlap the FROUNT binding surface. These results suggested that CCR2 Pro-C is not able to interact with both FROUNT and plasma membrane simultaneously.

To compare the binding affinity of CCR2 Pro-C to FROUNT and to the plasma membrane, we used SPR spectroscopy and NMR measurement. First, using SPR, we measured the affinity of CCR2 Pro-C to the plasma membrane, using liposomes that mimicked the lipid composition of natural plasma membrane. In this analysis, the interaction of the liposomes with CCR2 Pro-C was found to be dose dependent, and the dissociation constant for the interaction was calculated to be larger than that of the CCR2 Pro-C–FROUNT interaction (Terashima et al, unpublished data). These data suggested that CCR2 Pro-C interacts with membrane more weakly than with FROUNT. Next using NMR TCS experiments we examined the CCR2-binding properties of human FROUNT in the presence of a large excess of DPC micelles. The results revealed that FROUNT is able to bind to the hydrophobic surface in both the presence and absence of DPC micelles. These results suggested that CCR2 Pro-C is able to bind FROUNT even in the presence of plasma membrane.

Because CCR2 can interact with FROUNT only in response to chemokine stimulation, the CCR2—FROUNT interaction could be regulated by both chemokine stimulation and CCR2 activation. Taken together, we propose a CCR2-activation model in which a ligand-induced conformational change in CCR2 is required for FROUNT binding and downstream signaling. Pro-C has been revealed by mutational analyses to play an important role in the regulation of not only chemokine receptors but other GPCRs. Our studies may contribute to an understanding of a general pathway for GPCR regulation.

P-034 Construction and performance of a sample tube with a slot-shaped sample cavity fabricated within magnetic susceptibility-matched glass

Mitsuhiro Takeda[1], Klaas Hallenga[2], Masahiro Shigezane[3], Markus R. Waelchli[4], John L. Markley[2] and Masatsune Kainosho[1,5]
[1]Graduate School of Science, Nagoya University
[2]Department of Biochemistry, University of Wisconsin-Madison
[3] Shigemi Inc.
[4] Bruker Biospin K.K.
[5] Center for Priority Areas, Tokyo Metropolitan University

ABSTRACT
We describe the construction and performance of an NMR tube with a magnetic susceptibility-matched sample cavity. It confines the solution within the detection zone in the axial direction, and in a quasi-rectangular region in the radial direction. The slot-like sample cavity provides both good sample volume efficiency and tolerance to sensitivity loss in the sample space. The signal-to-noise ratio per unit volume of the constructed tube was 2.2 times higher than that of a cylindrical tube of 5 mm outer diameter, with a sample containing 300 mM NaCl at a static magnetic field of 14.1 T. Even the overall signal-to-noise ratio of the slot tube was 35% higher than that of the conventional 5 mm tube, for samples containing 300 mM NaCl. Similar improvements over existing sample tube geometries were obtained at 950 MHz. Moreover, the temperature increase resulting from RF heating was found to be significantly lower for the slot tube, even as compared to 3 and 4 mm outer diameter cylindrical tubes, as measured in a 5 mm cryoprobe. A further advantage of this type of tube is that a sample cavity of any desired size and shape can be formed within a cylindrical tube for use in a single cryogenic probe.

Ionic conductivity and dielectric losses with cryogenic probes at high magnetic field strengths severely limit the NMR sensitivity of aqueous solutions containing salt. When a cylindrical tube is placed in a Helmholtz probe, the magnitude of RF power dissipation varies widely within the sample space. In a radial cross section of the tube, the power dissipation increases with the distance from the center of the tube along a direction perpendicular to the B_1 field, resulting in the highest power dissipation at the edge regions.

Here we describe the design and construction of a cylindrical sample tube containing a slot-shaped sample cavity, fabricated from glass with magnetic susceptibility matching that of the sample solvent (SM-glass). The susceptibility-matched material serves as an alternative to the sample solvent, and can be used to form the intended sample space. In the slot tube design, the SM-glass confines the sample within the detection zone in the axial direction, as in a conventional Shigemi tube, and the two segment-shaped SM-glass pieces within the detection zone produce a quasi-rectangular-shaped sample cavity (Fig. 1). Overall, the quality of ^{1}H-1D NMR, 2D ^{1}H-^{15}N, and 2D ^{1}H-^{13}C spectra of the sample in the slot tube were nearly identical to those from the sample in a conventional Shigemi microtube.

Slot tube, Cryogenic probe, Salt-tolerance

We then compared the salt tolerance of the slot tube with that of a 5 mm microtube (Shigemi) and an oval-shaped tube (Bruker BioSpin), by measuring the SNRs of peaks in ^{1}H-^{15}N TROSY-HSQC spectra of 0.3 mM [U-^{13}C, ^{15}N]-ubiquitin samples, at NaCl concentrations of 0, 100, 200 and 300 mM and at static magnetic fields of 14.1 and 22.3 T. In the absence of added salt, the highest SNR was achieved with the 5 mm microtube. However, at the highest salt concentration (300 mM), a concentration frequently required to solubilize proteins, all three tube designs achieved comparable SNR values, with the slot tube and the oval-shaped tube slightly outperforming the 5 mm microtube at both 600 MHz and 950 MHz. Comparisons of the SNR per unit volume values demonstrate the clear advantages of the slot tube design over the two alternatives at all salt concentrations (Fig. 2). For example, at 600 MHz, for the protein solution containing 300 mM NaCl, the SNR per unit volume was over two times higher than those of the other designs.

When the performance of the slot tube was compared with those of three microtubes with 3, 4 and 5 mm outer diameters, the slot tube showed much lower heating over time and reached a steady state plateau earlier than the other designs. Since the heat conductivity of glass is larger than that of surrounding air, the sample heat appears to be dissipated more efficiently by the slot tube.

The slot tube exhibits practical advantages over alternative tube designs, in terms of SNR per unit volume and minimization of sample heating, particularly for samples containing high salt concentrations and data collected at high fields. Use of the slot tube can minimize the quantity, and hence the cost, of biomolecular samples. The slot tube can readily be introduced into normal laboratories at low cost, particularly when the probe is equipped with a sample positioning unit.

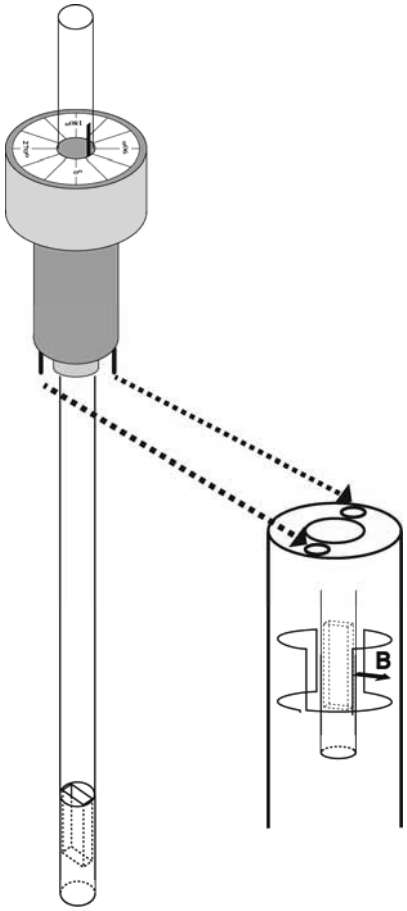

Fig. 1 The design of a slot tube. The tailored sample holder has two projections that insert into holes in the top of the probe, such that the tube is oriented to an intended angle

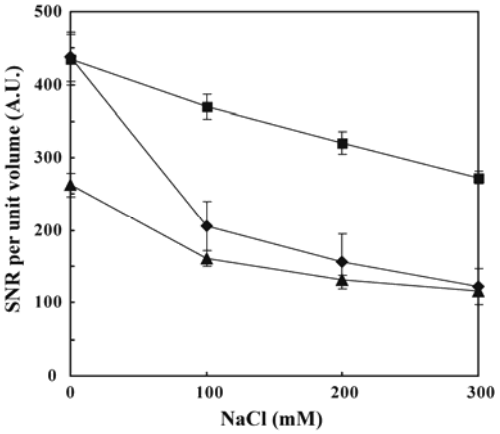

Fig. 2 SNR per unit volume at different salt concentrations at 14.1 T evaluated for the ubiquitin in the slot tube (■), 5 mm o.d. microtube (♦), and oval-shaped tube (▲)

Acknowledgements

This work was supported in part by the Targeted Protein Research Program (MEXT) and a Grant-in-Aid for Young Scientists (B) (21770110).

Reference

Takeda et al., *J. Magn. Reson.* **209**, 167-173 (2011).

P-035 Y

Elucidation of pyroglutamyl-amyloid beta peptides oligomerization mechanism by solution NMR analyses

Shigeto Iwamoto[1], Takashi Saito[2], Hitomi Yamaguchi[1], Toshiyuki Kohno[3], Takaomi C. Saido[2], Hiroaki Terasawa[1]
[1]Facul. of Life Sci., Kumamoto Univ., [2]RIKEN BSI,
[3]Mitsubishi Kagaku Inst., Life Sciences

ABSTRACT

Amyloid beta peptides (Aβ) oligomers, intermediates in the formation of amyloid fibrils, may be neurotoxic agents in Alzheimer's disease (AD) patients. N-terminal pyroglutamyl-Aβ (Aβ (3pE)) has been reported to be resistant to degradation and prone to aggregation. Moreover, senile plaques in AD patients are predominantly comprised of Aβ (3pE). In this study, we compared the aggregation propensities and structural differences between Aβ (3pE) and Aβ by NMR analyses. Our data showed that Aβ (3pE) may play a critical role in the formation of Aβ oligomers by forming a β-sheet and dynamic intermolecular interactions at the N-terminal regions.

[Introduction]

Aβ are thought to be neurotoxic polypeptides involved in AD, one of the most common pathology of late-onset dementia. It is estimated that 18 million people worldwide are living with a diagnosis of AD. Therefore, improved strategies for the prevention, earlier diagnosis and treatment of AD are desirable. Previously, it was said that the neurotoxicity of AD was caused by amyloid fibrils. However, recent physiological studies indicate that soluble Aβ oligomers, intermediates in the formation of amyloid fibrils, may possess significant neurotoxic properties. The main forms of Aβ found in amyloid deposits are 40 and 42 amino acids long and Aβ (1-42) displays enhanced neurotoxicity relative to Aβ (1-40). Additionally, pyroglutamate formation at the N-termini of Aβ enhances aggregation and confers resistance to aminopeptidases. Aβ (3pE) is formed by N-terminally truncation preceding the glutamate at position 3 and cyclization by the glutaminyl cyclase. Moreover, Aβ (3pE) were shown to constitute more than 50% of the Aβ in senile plaques in AD patients. The purpose of this study is to elucidate the role of Aβ (3pE) in the oligomerization process by NMR methods.

[Results and Discussion]

To obtain a stable isotope labeled peptide, Aβ was produced as ubiquitin fusion protein using *E. coli* to avoid aggregation. The ubiquitin can be removed by Yeast Ubiquitin Hydrolase (YUH) leaving no extra amino acid residues at the N-terminus of Aβ. The recombinant Aβ was then purified by reversed phase HPLC and characterized by MALDI TOF-MS. We similarly established a purification method for Aβ (3pE). In order to carry out the cyclization reaction, we deleted the first two amino acids at the N-terminus and mutated glutamate to glutamine at position 3. In addition, N-terminal cyclization was facilitated by phosphate buffer. Mass spectrometry analysis of Aβ confirmed the formation of N-pyroglutamyl.

Key words; Alzheimer's disease, Amyloid beta peptides, NMR

In order to investigate the structural differences between Aβ (3pE) and Aβ, we performed solution NMR analyses. First, we compared the ^{1}H-^{15}N HSQC spectrum of Aβ (3pE) with that of Aβ. Significant chemical shift differences were observed in the NMR signals of N-terminal regions, although these spectra closely resembled each other. These data indicate that the toxicity of Aβ (3pE) is related to local conformation of the N-terminus rather than global conformation. Moreover, the results of secondary structure prediction based on chemical shifts showed that the N-terminus of Aβ (3pE) has a greater tendency to form a β-strand than that of Aβ. Furthermore, temperature dependent intensity reduction of NMR signals derived from the N-terminal region of Aβ (3pE) is significantly larger to that of Aβ. These observations lead to the hypothesis that dynamic intermolecular interactions of the N-terminal regions correlate with the oligomerization of Aβ (3pE) and induce different oligomerization process compared with Aβ. To characterize the conformational exchange processes of Aβ, we measured ^{15}N longitudinal relaxation rate constants (R1) and ^{15}N $\{^{1}H\}$ heteronuclear NOE values. These data indicated that both Aβ (1-42) and Aβ (3pE-42) have flexible regions at their N-termini when assessing fast timescale (ps–ns) motions. The low NOE values were likely due to the rapid conformational dynamics between different conformations of Aβ at the ps – ns time scale.

To examine the effect of the N-terminal pyroglutamyl group on Aβ oligomerization, we performed the technique of Photo-Induced Cross-linking of Unmodified Protein (PICUP). Because the PICUP reaction requires very short time periods (less than 1 s) and occurs at neutral pH without the insertion of a spacer moiety or an unnatural photoreactive group, it is a useful method to elucidate metastable protein assembly characteristics. The results showed that Aβ (3pE-40) had a higher propensity to form small oligomers (dimers and trimers) compared to Aβ (1-40) without the formation of large oligomers. However, the oligomerization of Aβ (3pE-42) into high molecular weights was suppressed compared to that of Aβ (1-42). These data suggest that Aβ (3pE) may induce low molecular weight oligomers of Aβ (dimmers and trimers), which are presumed to be neurotoxic. Recently, we succeeded in extracting low molecular weight Aβ oligomers, stabilized by using PICUP. HPLC-fractionated Aβ monomer and Aβ oligomers were analyzed by SDS-PAGE and silver staining. It is possible to stabilize and isolate specific oligomers to determine structural features of Aβ oligomers and investigate whether a given oligomer is cytotoxic or not.

Our data show that Aβ (3pE) may play a critical role in the formation of Aβ oligomers by forming a β-sheet at the N-terminal regions and by the stacking of five-member rings in the pyroglutamyl group. Furthermore, Aβ (3pE) is assumed to promote oligomerization by dynamic intermolecular interactions of the N-terminal regions. Based on these data, we hypothesized that Aβ (3pE) may form oligomeric intermediates by intermolecular interactions of the N-terminal regions that are different from general Aβ oligomers. These properties of Aβ (3pE) may lead to small oligomer formation and neuronal toxicity.

[Perspective]

To determine the structural features of Aβ oligomers, we plan to perform NMR analyses of cross-linked stable Aβ and Aβ (3pE) oligomers. In addition, to obtain *in vivo* evidence that Aβ (3pE) plays key roles in AD, we will investigate the effect of intracerebroventricular injection of Aβ (3pE) oligomers and Aβ oligomers on the learning ability of rats. These results will provide valuable information for directing future efforts to treat AD.

P-036 Structure determination of the protein G B1 domain in living cells by in-cell NMR spectroscopy

Saori Hosoya[1], Tomomi Hanashima[1], Junpei Hamatsu[1], Teppei Ikeya[1], Masaki Mishima[1], Peter Güntert[2], Masahiro Shirakawa[3] and Yutaka Ito[1]
[1]Dept. of Chem., Tokyo Metropolitan Univ., [2]Inst. of Biophysical Chemistry and Center for Biomolecular Magnetic Resonance, J. W. Goethe-Univ. Frankfurt, [3]Dept. of Eng., Univ. of Kyoto

[Abstract]

Recently we reported the first three dimensional (3D) protein structure calculated exclusively on the basis of information obtained in living *E.coli* cells. We are currently addressing the structure determination of the protein G B1 domain (GB1) overexpressed in *E. coli* cells as an another demonstration of our approach. The GB1 in-cell NMR samples suffer from lower intracellular concentration (0.25-0.5 mM), thus further methodological optimisation was required for resonance assignments, NOE analysis and structure calculation. In this presentation we report the GB1 in-cell structure as well as our modified NMR methods.

[Introduction]

Recent developments in NMR hardware and methodology have enabled the measurement of high-resolution heteronuclear multi-dimensional NMR spectra of macromolecules in living cells (in-cell NMR). With this method, we achieved the first three dimensional (3D) protein structure determination using nonlinear sampling, selective protonation at methyl groups, etc.[1,2] Despite various applications of the approach being expected, however, the second in-cell structure so far has not been presented, presumably because of the requirement of preparing stable samples with high intracellular protein concentration.

We are currently addressing the structure determination of the *Streptococcus* protein G B1 domain (57 a.a., GB1) in *E. coli* cells as an another demonstration of our in-cell NMR approach. Although the protein is relatively stable and yields high-resolution in-cell spectra, the concentration is approximately 10 times lower than for our first target, which makes the assignment, particularly of the sidechains, difficult. Very recently, two computational methods have been proposed for spectral data processing and fully automated assignment, respectively. As the processing of non-linearly sampled spectral data that is necessary for in-cell NMR, a new maximum entropy reconstruction (MaxEnt) software was released by Laue et al., which automatically determines the optimal noise level based on probability theory. The improved MaxEnt algorithm is expected to overcome the difficulty of the noise level determination in the in-cell spectra, where due to inconsistent signal-to-noise ratios some regions are crowed with peaks and noise but others are sparse with less noise. As an automated assignment method, on the other hand, an exclusively NOESY-based approach has been proposed.[3] While triple resonance spectra for the backbone assignment and the ^{13}C,^{15}N-NOESY spectra of GB1 show relatively strong and separated peaks, the ones for the sidechain assignment suffer from low intensities. Thus it was not trivial to accomplish the manual sidechain assignment. The two NOESY spectra are well resolved, such that they potentially contain the information for the resonance assignment of the sidechains, the exclusively NOESY-based method may result in additional chemical shift assignments and a more accurate structure. Here we show the current progress of the in-cell NMR structure determination of GB1 and the feasibility of the two novel methodologies for applications to in-cell NMR data.

In-cell NMR, Heteronuclear multi-dimensional NMR, Structure determination

[Methods]

E. coli cells harbouring the plasmid encoding the GB1 gene were first grown in unlabelled LB medium. Protein production was induced after transfer of the bacteria into stable isotope-labelled medium. The collected cells were placed as a 60% slurry into NMR tubes. Sample stability was monitored repeatedly by 2D $^{1}H–^{15}N$ HSQC spectra followed by plating colony tests. Rapid measurement of the 3D NMR spectra by nonlinear sampling of the indirectly acquired dimensions was used to overcome problems caused by the instability and low sensitivity of living *E. coli* samples. For the collection of NOE-derived distance restraints, 3D ^{15}N-separated and ^{13}C-separated NOESY-HSQC spectra were measured on ^{13}C and ^{15}N labelled in-cell NMR samples.

[Results]

Backbone and side-chain NMR resonance assignments of GB1 in living cells were performed by manually analysing 3D triple-resonance NMR spectra. The H^N, N, C^α, H^α and C' resonances of the backbone were almost completely assigned (Fig. 1). The improved MaxEnt algorithm was applied to the triple resonance spectra mainly for the sidechain assignment and the ^{15}N,^{13}C-separated NOESY-HSQC. It notably enhances the signal-to-noise ratio, and recovers approximately 30% of the missing signals in the spectra processed by conventional MaxEnt of the program AZARA (Fig. 2). Consequently, 58% of the sidechain resonances were manually assigned from those spectra.

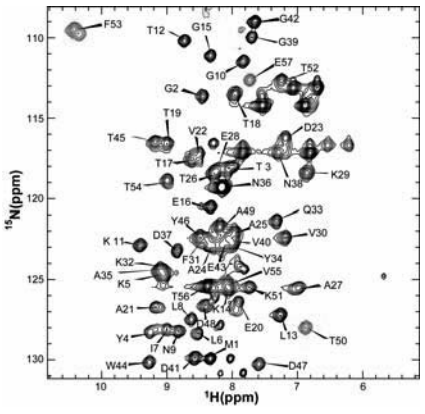

Fig. 1 2D ^{1}H-^{15}N HSQC spectrum of the ^{13}C/^{15}N-labelled GB1 in living *E.coli* cells. Cross peaks are labelled with their corresponding backbone assignments.

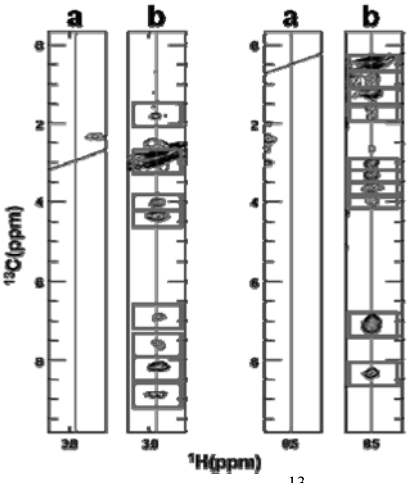

Fig. 2 Comparing of ^{13}C-separated NOESY-HSQC processed by the conventional MaxEnt of AZARA (a) and improved one (b). Squares on the slices denote additionally obtained peaks by the improved MaxEnt.

Although the spectra for the sidechain are improved by the elaborate MaxEnt processing, the assignments are still not sufficient for getting high resolution 3D structures. Thus, the exclusively-NOESY based automated assignment method is employed in order to utilize the ^{15}N, ^{13}C-NOESY as supporting information for the sidechain assignment. Since the two NOESYs are complicated by broad lines and artifacts compared to those of the previous report that was entirely done with no user intervention[3], the manually assigned chemical shifts and primitive structures derived from them are adopted as prior information. Here we demonstrate the improvement by those computational methods and the feasibility of accurate protein structure determination for proteins with low intracellular protein concentration in the cells.

[References]

1) Sakakibara D., Sasaki A., Ikeya T., Hamatsu J., Hanashima T., Mishima M., Yoshimasu M., Hayashi N., Mikawa T., Wälchli M., Smith O. B., Shirakawa M., Güntert P. and Ito Y., *Nature* 458, 102-105 (2009)

2) Ikeya T., Sasaki A., Sakakibara D., Shigemitsu Y., Hamatsu J., Hanashima T., Mishima M., Yoshimasu M., Hayashi N., Mikawa T., Nietlispach D., Wälchli M., Smith O. B., Shirakawa M., Güntert P. and Ito Y., *Nature Protocols* **5**, 1051–1060 (2010)

3) Ikeya, T., Jee. J. G., Shigemitsu, Y., Hamatsu, J., Mishima, M., Ito, Y., Kainosho, M. & Güntert, P., *J. Biomol. NMR*.**50**, 137-146 (2011)

P-037 Structure, dynamics and function of high-energy state mutant of ubiquitin

Soichiro Kitazawa [1], Maho Yagi-Utumi [2,3], Akemi Ido [5],Makoto Urushitani [5], Kenji Sugase [4], Koichi Kato [2,3] and Ryo Kitahara[1]
[1] College of Pharmaceutical Science, Ritsumeikan University (Japan),
[2] Okazaki Institute for Integrative Bioscience and Institute for Molecular Science, National Institutes of Natural Sciences (Japan), [3] Graduate School of Pharmaceutical Sciences, Nagoya City University (Japan), [4] NMR Group, Division of Organic Chemistry, Bioorganic Research Institute, Suntory Foundation for Life Sciences (Japan) and [5] Shiga University of Medical Science, Molecular Neuroscience Research Center (Japan)

We demonstrate a rational design for the high Gibbs-free energy conformer N_2 of ubiquitin based on the solution structure of the N_2 state of the wild-type protein, previously characterized by high pressure NMR spectroscopy. We created the ubiquitin mutant as the first model of a stable high-Gibbs energy state of ubiquitin, N_2. Structure, dynamics and stability of the N_2 state are characterized by ^{1}H, ^{15}N, ^{13}C chemical shifts, ^{15}N-spin relaxation, water-amide proton exchange (CLEANEX-PM) and RDC experiments. The ubiquitin mutant represents structural features similar to that observed for the N_2 state of the wild type protein. We also examined functional activity of the mutant in terms of its interaction with the ubiquitin interacting motif UIM and polyubiqutination through the E1-E2-E3 cascade reactions.

Introduction

Conformational fluctuations are considered to be important for protein functions. Recently, a variety of approaches by solution NMR spectroscopy such as R_2 dispersion, residual dipolar coupling and high pressure NMR have demonstrated a presence of high-Gibbs-free energy states of a protein. However, atomic level detailed structural studies of these high-energy states are still limited because the high-energy conformers are often less populated and invisible by NMR at physiological temperature and pressure. Previously, by using high pressure NMR spectroscopy, we found two high-energy states (alternative form N_2 and locally disordered form I) of the protein equilibrium with the basic folded sate and totally unfolded state. Moreover, we determined the solution structure of the N_2 state at 3 kbar, giving NMR snapshots of a fluctuating protein structure at atomic resolution (Fig. 1) (1). The result revealed that the helix swings out with simultaneous reorientation of the C-terminal segment, providing an open conformation suitable for enzyme recognition. Intriguingly, such high-energy states are conserved in ubiquitin and ubiquitin-like proteins (NEDD8 and SUMO-2) (2,3) that have common functional strategy, the E1-E2-E3 cascade reactions. These results strongly suggested that the N_2 state could be involved in the function of ubiquitin binding or ubiquitination reactions. Here, we report characterization in structure and dynamics of the ubiquitin mutant.

Keywords: ubiquitin, high-energy state, pressure, CLEANEX, residual dipolar couplings

Results and Disucussion

In order to obtain NMR signal assignments for backbone and side-chain atoms, we carried out a series of triple resonance experiments for ^{13}C and ^{15}N uniformly-labeled mutant of ubiquitin on DRX-600 spectrometer. Large chemical shifts by mutation are observed at residues located at C-terminal side of the protein, indicating a large population of the high-energy N_2 state in the protein.

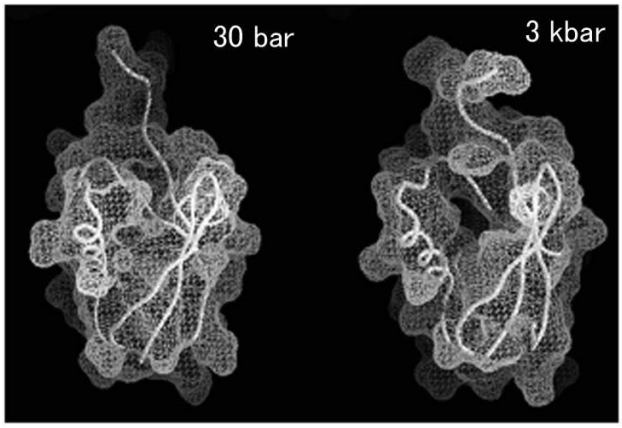

Figure 1. Molecular surface of wild-type ubiquitin at 30 bar and at 3 kbar corresponding to the N_1 and N_2 states of the protein, respectively.

Residual Dipolar couplings (RDC) of backbone N-H vectors for WT and mutant were also measured in solution with Pf1 bacteriophage. Alignment tensor parameters calculated by the program MODULE2 indicate that structure of the mutant is similar to WT in large part, but relative orientations of the C-terminal regions are remarkably changed in the mutant protein. ^{15}N transverse relaxation rate constants R_2 of backbone amide groups for WT and mutant are obtained at three external magnetic fields, ^{1}H 600 MHz, 750 MHz and 950 MHz. The relaxation analysis suggests that conformational fluctuation takes place at the C-terminal side of the protein at μs-ms time scale. In addition, water-amide proton exchange analysis by the clean chemical exchange (CLEANEX-PM) NMR spectroscopy showed that the C-terminal side of the mutant has faster exchange rates than those in WT. Since many of the residues showing large R_2 and fast water-amide proton exchange rates are involved in the conformational transition from N_1 to N_2, the mutant would favor the population of the N_2 state. These results clearly show that the mutant is a reasonable model of the N_2 conformer of ubiquitin and useful for further structural and functional studies of ubiquitin and ubiquitin related systems.

Refarence

1. Kitahara, R. et al. *J. Mol. Biol.* **2005**, 347, 277-285.
2. Kitahara, R. et al. *J. Mol. Biol.* **2006**, 363, 395-404.
3. Kitahara, R. et al. *Biochemistry* **2008**, 47, 30-39.

P-038 Base-deamination rate dependent on the direction of sliding of an enzyme along DNA as revealed by numerical analysis of NMR data, and wood biomass studied by solution NMR

Hiroshi Nishimura[1], Ayako Furukawa[1], Hideyasu Okamura[1], Yu Kozawa[1], Ryo Morishita[2], Akihide Ryo[3], Kenji Sugase[4], Takashi Watanabe[5], and Masato Katahira[1]
[1]Inst. of Advanced Energy, Kyoto Univ., [2]CellFree Sci., [3]Grad. Sch. Med., Yokohama City Univ., [4]Bioorg. Res. Inst., Suntory Found. Life Sci., and [5]RISH, Kyoto Univ.

Abstract

We have developed a new method for the preparation of the solution NMR sample of whole wood. This method gives much sharper line width. Complete HSQC/HMQC correlations can be obtained for key biomass materials contained in the whole wood, such as a dibenzodioxocin form of lignin, thanks to much better resolution of the corresponding spectra. Thus, this method contributes to the identification of the key materials in the whole wood. Additionally, several exchangeable protons such as a phenolic one become visible with this preparation method. $^{1}J_{CH}$ values were determined for various composition units of the wood biomass with TROSY. These values can be used to quantify the amount of those units based on the HSQC spectrum. Secondly, numerical analysis of the location-dependent base-deamination rate by anti-HIV APOBEC3G along DNA has suggested that the reaction rate depends on the direction of sliding of APOBEC3G. Thirdly, the structural analysis of the flexible N-terminal half (107 a.a.) of prion protein in complex with RNA aptamer has revealed how this aptamer traps the prion protein with high affinity.

Wood Biomass

We have found that the decantation of the milled wood and the addition of metal ions improve the quality of NMR spectra. ^{1}H-^{13}C HSQC spectra of whole Japanese beech samples prepared in a conventional way (Figure 1b) and in a newly developed way (Figure 1c) are compared. Apparently, the sample prepared in the newly developed gives much sharper spectrum. Thanking to much better resolution of the spectrum, key biomass materials can be identified in a straightforward way with HSQC and HMBC spectra. For example, a dibenzodioxocin form of lignin (chemical structure F in the upper right of Figure 1), which is a critical composition unit for the formation of the branch structure of lignin, can be readily identified in HSQC. Furthermore, complete HSQC/HMBC correlation of the dibenzodioxocin form has been obtained for the first time in the whole wood. It was revealed that this new method makes several exchangeable proton signals such as a phenolic one visible, which also contributes to the identification of key biomass materials.

$^{1}J_{CH}$ values were determined for various composition units of the wood biomass with TROSY. It was found that the values vary from 120 to 170 Hz for materials contained in the whole wood. By taking into account the variation of $^{1}J_{CH}$ values, the amount of the key biomass materials can be precisely quantified on the basis of HSQC spectrum.

Sliding-Direction-Dependent Deamination Rate

We have already reported that a cytidine located closer to the 5' end of ssDNA is deaminated by an anti-HIV factor, APOBEC3G, faster than that located less close to the 5' end on the basis of real-time monitoring of the enzymatic reaction with NMR. Here, the numerical analysis of the experimental data has suggested that the reaction rate depends on the direction of sliding of APOBEC3G on ssDNA: APOPBEC3G pointing toward the 5' direction deaminates a cytidine more effectively than that pointing toward the 3' direction.

N-Terminal Half of Prion Protein in Complex with RNA Aptamer

Structural analysis the N-terminal flexible half of prion protein (107 a.a.) in complex with RNA aptamer has revealed that two binding regions of the prion protein bind to the top and the bottom of the dimeric structure of RNA aptamer in a fast exchange mode without complete dissociation from the aptamer. This rationalizes the high affinity of RNA aptamer against prion protein.

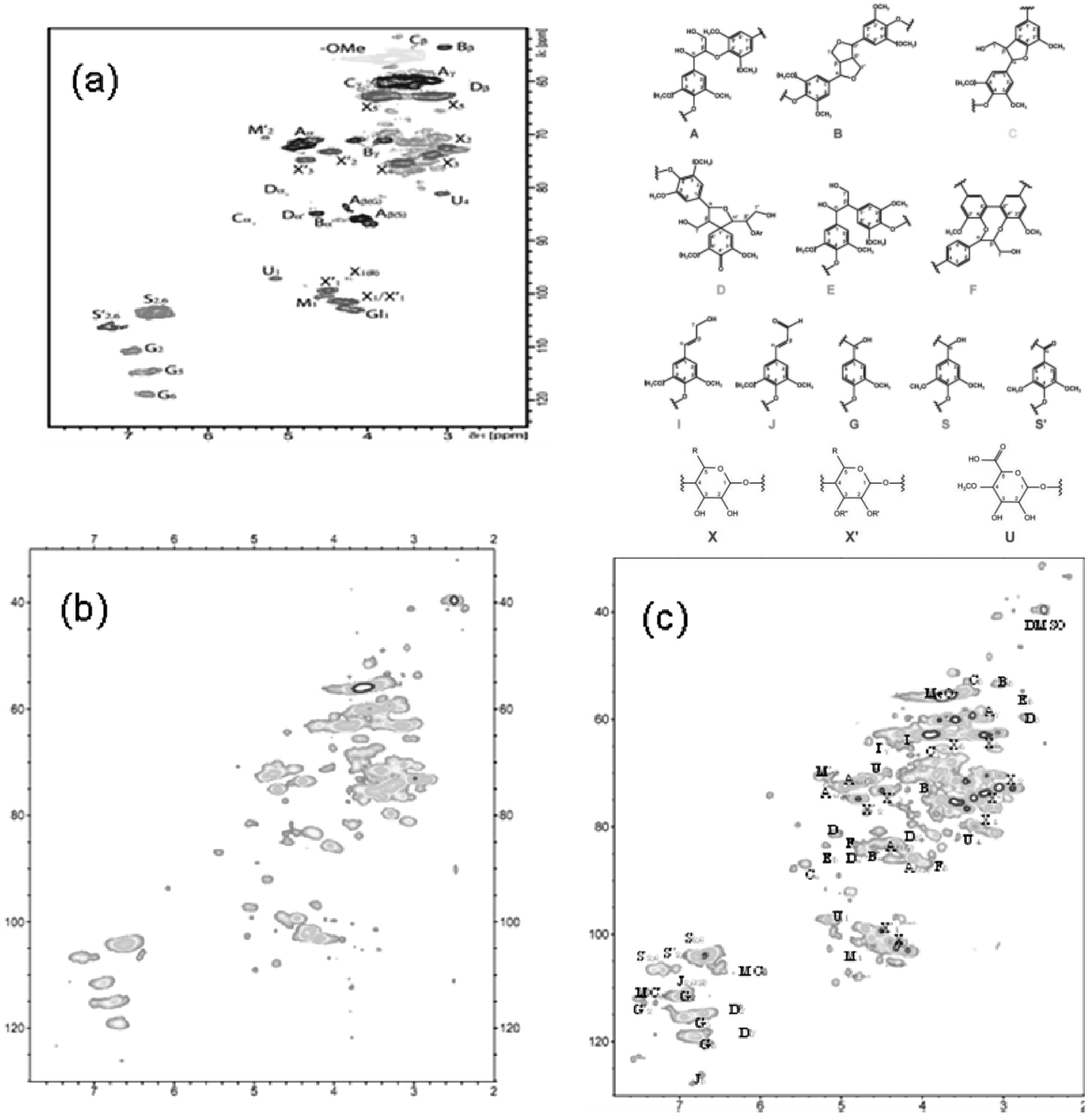

Figure 1 Comparison of ^{1}H-^{13}C HSQC spectra of whole wood. (a) Whole *Eucryphia cordifolia* sample prepared in a conventional way (Martinez *et al.*, Environ. Microbiol., 13, 96-107, 2010). (b) Whole *Japanese beech* sample prepared in a conventional way. (c) Whole *Japanese beech* sample prepared in a newly developed way. Chemical structures of composition units of lignin and cellulose of the whole wood are shown in the upper right.

Biomass, Lignin, Sliding

P-039 NMR analyses of mouse peptide ESP4 to elucidate structure and Ligand - receptor recognition mechanisms

Masahiro Taniguchi[1], Sosuke Yoshinaga[1], Sachiko Haga[2], Kazushige Touhara[2] and Hiroaki Terasawa[1]
[1]Graduate School of Pharmaceutical Sciences, Kumamoto University
[2]Graduate School of Agricultural and Life Sciences, The University of Tokyo

Abstract

Pheromones are chemical substances that convey information about social and reproductive behaviours in the same species. Pheromones can be discriminated accurately, but the details of the specific mechanism are yet to be understood. We previously identified a sex-specific pheromone ESP1, expressed in male mouse tear fluids. ESP1 and ESP4 are regulated by a multigene peptide producing family which consists of 38 genes in mice. ESP4 has the highest homology with ESP1 among the members of the ESP family and is expressed in three exocrine glands of both male and female mice. The aim of this study is to elucidate the specific ligand-receptor recognition mechanism of ESP4. We performed biological and NMR analyses of ESP4. We discuss the structure-activity relationship of ESP4 and ESP1. In addition, we constructed some mutants to suppress the unfavorable aggregation. We also report the results of NMR analyses about the mutants.

Introduction

Pheromones are chemical substances that convey information about social and reproductive behaviours in the same species. In mammals, especially rodents, pheromones are detected through vomeronasal sensory neurons (VSNs) in the vomeronasal organ (VNO) located in nasal cavity. Pheromones can be discriminated accurately between the same species. To understand the discrimination among the cognate species, it is important to reveal the mechanism of specific ligand-receptor recognition .

Recently, we identified a male-specific peptide from the extraorbital lacrimal gland (ELG) and named the peptide exocrine gland-secreting peptide 1 (ESP1) [1)]. ESP1 and ESP4 are regulated by a multigene peptide producing family which consists of 38 genes in mice[2)]. ESP4 has the highest homology (43% identity) with ESP1 among the members of the ESP family and is expressed in the ELG, the Harderian gland and the submaxillary gland of both male and female mice.

No peptide pheromone receptors have been identified except for the ESP1 receptor and now the analyses of the ligand-receptor recognition are in progress. We previously determined the structure of ESP1, identified the ESP1 receptor and elucidated the function that ESP1 enhances female sexual behaviour. But for the other ESP family proteins, no information about the structure and the receptor is available.

The purpose of this study is to clarify the specific ligand-receptor recognition mechanism of ESP4, based on biological and structural analyses.

pheromone, ESP family, specific ligand-receptor recognition

Materials and Methods

Uniformly $^{13}C/^{15}N$- and ^{15}N-labelled proteins were prepared by growing *Escherichia coli* strain BL21(DE3) cells in M9 medium. ESP4 was purified through Ni-chelate affinity chromatography and reversed-phase chromatography. The identity and the integrity of all of the purified proteins were confirmed by MALDI/TOF MS and SDS-PAGE. The induction of c-Fos expression was examined as a marker for activated VSNs and double-immunostaining of VNO sections collected from ESP1- and ESP4-stimulated mice labeled with anti-ESP1 receptor protein and anti-c-Fos antibodies was carried out. NMR measurements were performed at 35 ºC using a Bruker Avance 600 or Avance 500 spectrometer with a cryogenic probe. NMR data were processed using the NMR Pipe program and analysed using the Olivia program. The NOE peak assignments and the structural calculations were performed using the CYANA program.

Results and Discussions

The double-immunostaining with anti-ESP1 receptor protein and anti-c-Fos antibodies indicated that all ESP1-activated and c-Fos-positive neurons expressed the ESP1 receptor protein, while ESP4 induced c-Fos expression that were negative for the ESP1 receptor. The results suggested that ESP4 receptor is different from ESP1 receptor.

For determination of the three-dimensional structure of ESP4, we completed the backbone and side chains assignments of ESP4 by ^{1}H, ^{13}C and ^{15}N triple resonance spectra. The heteronuclear NOE values showed that both ESP4 and ESP1 have highly flexible regions at the N-termini. SSP (secondary structure propensity) scores and distance information obtained from 3D NOESY spectra suggested that ESP4 has four helices, while ESP1 consists of three helices. The fourth helix at the C-termini of ESP4 is major structural difference, compared with the ESP1 structure.

Next we focused on electrostatic surface potentials of ESP4. Based on the NMR structural analyses, we found that the electrostatic surface potentials of ESP1 and ESP4, which are important for the VSNs-stimulating activity of ESP1, are quite different (Fig. 1). For example, the ESP1 surface is characteristically rich in positive charges on the first helix, while the ESP4 surface is rich in negative charges on the first helix.

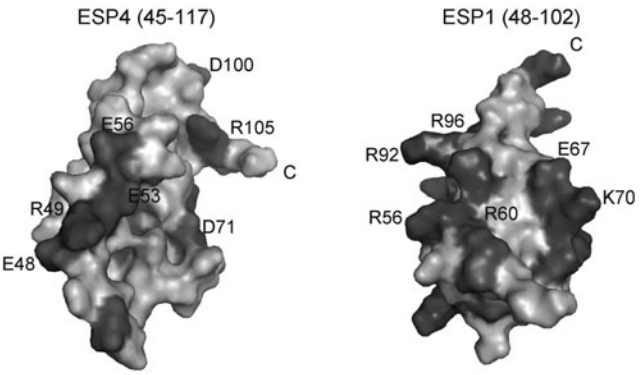

Fig. 1 Comparison of ESP4 and ESP1 structures. Electrostatic surface potentials of ESP4 are different from those of ESP1.

The differences in the electrostatic surface potentials and the additional helix at the C-termini may play an essential role in the specific receptor recognition of ESP4 and ESP1.

Besides these analyses, we newly conducted titration experiments to identify the aggregation site and constructed some mutants to suppress the aggregation. We discuss the strategy and NMR analyses of the mutants.

References

[1] Kimoto H. *et al.*, *Nature,* **437**, 898-901 (2005)

[2] Kimoto H. *et al.*, *Current biology*, **17,** 1879-1884 (2007)

P-040 NMR studies on the Chp1 chromodomain

Hideaki Shimojo[1], Mayumi Ishida[2,3], Jun-ichi Nakayama[2,3], and Yoshifumi Nishimura[1]

[1]Department of Supramolecular Biology, Graduate School of Nanobioscience, Yokohama City University
[2]Laboratory for Chromatin Dynamics, RIKEN Center for Development Biology
[3]Department of Bioscience, Graduate School of Science and Technology, Kwansei-Gakuin University

Assembly of heterochromatin at centromeric DNA regions in the fission yeast requires the RNA-induced transcriptional silencing (RITS) complex, which consists of Chp1, Ago1, Tas3, and centromeric siRNAs. Chp1 contains chromodomain, which is known to be a methyl-lysine recognition or RNA/DNA binding module. The binding of the Chp1 chromodomain to methylated lysine 9 of histone H3 (H3K9me) is crucial for the efficient establishment of centromeric heterochromatin. We determined the solution structure of the Chp1 chromodomain bound to H3K9me.

INTRODUCTION

In eukaryotes, the formation of silent chromatin or heterochromatin is critical for a variety of cellular processes including global regulation of gene expression, centromere and telomere function, dosage compensation, and the maintenance of genomic stability. Posttranslational modifications of histone tails, catalyzed by histone-modifying enzyme, organize chromosomes into functionally distinct domains, active or inactive domains.

The maintenance of centromeric heterochromatin in fission yeast relies on the RNA interference-dependent complexes RITS (RNA-induced transcriptional silencing complex) and RDRC (RNA-directed RNA polymerase complex), which cooperate in a positive feedback loop to recruit high levels of histone H3 K9 methyltransferase activity to centromeres and to promote the assembly and maintenance of centromeric heterochromatin.

Chromodomains, originally identified in heterochromatin-associated factors, are considered as modules used to target proteins to specific chromosomal loci. The chromodomain family display a range of activities, including methyl lysine recognition, and RNA / DNA binding.

In fission yeast, the key factors for the assembly of centromeric heterochromatin, Chp1, Chp2, Clr4, and Swi6, have a chromodomain. The chromodomain of Chp1 is crucial for tethering the RITS complex to centromeric regions. The Chp1 chromodomain bound to H3K9me is essential for the establishment of heterochromatin.

Chp1, chromodomain, solution structure

METHOD

The recombinat Chp1 chromodomain was expressed E.coli using pCold system and purified by Ni-NTA and gel-filtration column chromatography. For resonance assignment of the chromodomain various 3D NMR spectra were obtained. All spectra were processed by program NMRPipe and analyzed by program Olivia. Structure was calculated by program CYANA. The histone peptide and RNA titration experiments were performed by NMR and ITC.

RESULT

We determined the solution structure of the Chp1 chromodomain complex with a trimethylated lysine 9 H3 peptide (H3K9me3). The overall core structure is same to the crystal structure which was already reported. Compare to the crystal structure, we used a 20 amino acids longer construct in N-terminal region, where a short 3^{10} helix was formed in NMR structure.

Recently it was suggested that the Chp1 chromodomain binds to ssRNA. Here, we identified the shifted residues of the Chp1 chromodmain by binding to ssRNA and the Kd value using NMR. The Chp1 chromodomain bind to RNA. It is suggested that the binding of ssRNA and H3K9me3 to the Chp1 chromodomain are independence between ssRNA and H3K9me binding. The interacting amino acids of thee Chp1 chromodomain with ssRNA are required to the Chp1 chromodomain function in RNAi-mediated heterochromatin assembly.

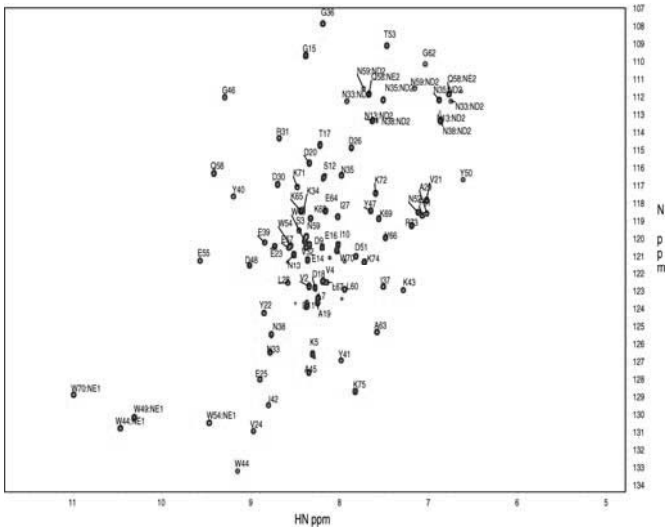

Figure.1 2D 1H-15N HSQC spectrum of the chromodomain of the Chp1

Figure.2 The solution structure of the Chp1 chromodomain H3K9me3 complex